Title: Myc and Tor drive growth and cell competition in the regeneration blastema of *Drosophila* wing imaginal discs

Running title: Myc and Tor in Regeneration

Felicity Ting-Yu Hsu[1] and Rachel Smith-Bolton[1]

[1] Cell and Developmental Biology, University of Illinois at Urbana-Champaign, Urbana, IL 61801, USA

*Author for correspondence (rsbolton@illinois.edu)

Keywords: Regeneration, Drosophila, Myc, Tor, Cell Competition

Summary statement

Drosophila wing disc regeneration is characterized by concentric growth zones controlled by the Myc transcription factor, the Tor signaling pathway, and Myc-induced cell competition.

Abstract

During the regeneration of injured or lost tissues, the regeneration blastema serves as a hub for robust growth. *Drosophila* imaginal discs are a genetically tractable and simple model system for the study of regeneration and organization of this regrowth. Key signals that contribute to regenerative growth in these discs, such as ROS, Wnt/Wg, JNK, p38, JAK/STAT, and the Hippo pathway, have been identified. However, a detailed exploration of the spatial organization of regrowth, the factors that directly drive this growth, and the consequences of activating drivers of regeneration has not been undertaken. Here, we find that regenerative growth in imaginal discs is controlled by the transcription factor Myc and by Tor signaling, which drive proliferation and translation in the regeneration blastema. The spatial organization of growth in the blastema is arranged into concentric growth zones defined by Myc expression, elevated Tor activity, and elevated translation. In addition, the increased Myc expression in the innermost zone induced Xrp1-independent cell competition-like death in the adjacent zones, revealing a delicate balance between driving growth and inducing death in the regenerating tissue.

Introduction

Regeneration is a phenomenon through which some animals restore tissues or organs after damage. This regrowth often occurs through proliferation of a group of undifferentiated and robustly growing cells at the damage site, called a blastema (reviewed in Londono et al., 2018). To study tissue regeneration, we use *Drosophila* wing imaginal discs as a model. The ability of these appendage primordia to regenerate during the larval stage was discovered when the imaginal discs were cut and incubated in the abdomens of female flies (Hadorn and Buck, 1962). Two decades later, blastema-like cells were found robustly proliferating at the wound site in leg and wing imaginal discs (Abbott et al., 1981; O'Brochta and Bryant, 1987). Subsequent searches for signaling pathways important for regenerative growth identified Jun N-terminal Kinase (JNK) signaling as crucial for disc regeneration after fragmentation (Bosch et al., 2005), and lineage tracing demonstrated that cells experiencing JNK signaling were the origin of the regeneration blastema (Bosch et al., 2008). More recently, genetic ablation systems have replaced fragmentation in regeneration studies, where localized massive cell death is generated through overexpression of pro-apoptotic genes (Fox et al., 2020). In these ablation systems, blastema cells were also found around the wound sites during regeneration (Smith-Bolton et al., 2009). To better define the blastema, two research groups (Floc'hlay et al., 2023; Worley et al., 2022) used single-cell RNA-sequencing (scRNA-seq) to characterize blastema cells by gene expression. This approach identified two clusters of cells with expression of signaling molecules such as Wg and Upd3 and transcription factors such as Ets21C that define the blastema (Floc'hlay et al., 2023; Worley et al., 2022). However, gene expression alone may not capture all changes in cell behavior and may not identify all cells contributing to the regenerating tissue.

During normal development, low ecdysone levels maintain larval development and growth of the imaginal discs, while a burst of high ecdysone production triggers developmental transitions such as molting or pupariation (Thummel, 2001). The ability of imaginal discs to form a blastema is reduced during the late third instar due to an increase in the hormone ecdysone, which silences damage-responsive signals (Halme et al., 2010; Harris et al., 2016; Jaszczak and Halme, 2016). Damage during the early- and mid-third

larval instar induces secretion of the relaxin-like peptide *Drosophila* insulin-like peptide 8 (dILP8), which reduces systemic ecdysone and delays the surge to prolong larval development. This reduced ecdysone also reduces imaginal disc growth outside of the damaged area (Colombani et al., 2012; Garelli et al., 2012; Halme et al., 2010; Jaszczak and Halme, 2016; Jaszczak et al., 2015; Jaszczak et al., 2016; Karanja et al., 2022; Katsuyama et al., 2015). Therefore, the regeneration blastema must override the global reduction of growth due to low ecdysone levels.

In this paper, we demonstrate that the transcription factor Myc and the Target of Rapamycin (Tor) signaling pathway drive blastema growth. Both Myc transcription and Tor signaling were upregulated during regeneration. Reducing their expression or kinase activity reduced proliferation and translation in the blastema. Interestingly, the area with activated Tor signaling extended beyond the area with high Myc expression, establishing concentric zones of blastema growth.

Cell competition occurs when neighboring cells have different fitness levels, and “loser cells” are eliminated by cell death, while “winner cells” replace the loser cells. Differences in Myc expression between adjacent cell populations lead to cell competition or super-competition during normal development (De La Cova et al., 2004; De La Cova et al., 2014; Meyer et al., 2014; Morata, 2021). More specifically, cell competition occurs when wild-type cells are winners and cells with reduced Myc expression are losers, and super-competition occurs when cells with elevated Myc expression are winners and wild-type cells are losers (Reviewed in Morata, 2021). Death of the loser cells can involve autophagy (Nagata et al., 2019) and expression of the transcription factor Xrp1 (Baillon et al., 2018; Blanco et al., 2020; Kiparaki et al., 2022; Lee et al., 2018; Ochi et al., 2021).

Proteotoxic stress, as assessed by increased levels of phosphorylated eIF2α, has been reported in loser cells during cell competition (Baumgartner et al., 2021), and phosphorylated eIF2α is sufficient to induce loser cell fate (Kiparaki et al., 2022). However, increased phosphorylation of eIF2α also occurs in winner cells during super-competition, although these cells are protected from this proteotoxic stress and do not undergo

apoptosis (Paul et al., 2024). Thus, eIF2α phosphorylation can be used to distinguish between cell competition and super-competition. In addition, several mechanisms can play a role in the comparison of cell fitness during various forms of cell competition (Morata, 2021; Nagata and Igaki, 2024), including Spätzle/Toll signaling (Alpar et al., 2018; Germani et al., 2018; Meyer et al., 2014) and Flower/Azot signaling (Merino et al., 2015; Rhiner et al., 2010). These mechanisms that govern cell competition in wing imaginal discs have predominantly been studied using induced clones of genetically distinct cell populations (Reviewed in Khandekar and Ellis, 2024). Whether the Myc expression differences that arise during regeneration also lead to competitive behaviors and whether the underlying mechanism aligns with any of the established models of cell competition were unclear.

Here, we show that cell death is increased in the cells adjacent to the high Myc-expressing cells in the blastema. Furthermore, this cell death was suppressed when Myc expression was eliminated, indicating the presence of cell competition. The cells adjacent to the high-Myc cells showed an increase in autophagy and eIF2α phosphorylation, similar to loser cells in cell competition. However, we did not find elevated Xrp1 expression, and heterozygosity for Xrp1 did not eliminate Myc-induced cell death in regenerating wing discs. In addition, the known fitness comparison mechanisms were not active. Therefore, the heterogeneity and complex signaling in the regeneration blastema likely leads to a type of cell competition that is not identical to the competition induced when two sets of cells differ by only one factor. The finding that wing disc regeneration involves not only robust regrowth but also increased cell death suggests that there is a dynamic balance between growth and death, providing new insights into the microenvironment of regenerating tissue.

Results

Myc and Tor drive blastema growth

To study regeneration in the *Drosophila* wing imaginal disc, we used a genetic ablation system in which tissue damage can be induced with spatial and temporal precision (Smith-Bolton et al., 2009). This ablation system uses the UAS/Gal4 transcriptional

132 system, where a Gal4 in the *rotund* (*rn*) locus directs the expression of the pro-apoptotic
133 gene *reaper* (*rpr*) in the wing imaginal disc pouch (Fig. 1A). In addition, the Gal4 activity
134 is constrained by Gal80^{ts} at 18°C but not at 30°C. We raised the larvae in an 18°C
135 incubator for seven days after egg-laying, when the larvae reach the early third instar
136 stage, then transferred the larvae to a 30°C water bath for 24 hours to activate apoptosis.
137 After the 24-hour temperature shift, the larvae were returned to 18°C. This time point was
138 considered recovery time 0 (R0) (Fig. 1A).
139
140 To characterize growth in a regenerating wing disc, we examined proliferation in
141 undamaged and regenerating discs 24 hours after the end of tissue damage, or recovery
142 time 24 (R24). We used EdU incorporation to mark cells in S-phase and anti-phospho-
143 histone H3 (PH3) immunostaining to mark cells in mitosis. We compared the undamaged
144 wing pouch, whose outer edge is marked by the inner ring of Wg expression (Fig.
145 S1A,A')(Swarup and Verheyen, 2012), and the regeneration blastema, which is marked
146 by Wg expression throughout (Fig. S1B,B') (Smith-Bolton et al., 2009; Worley et al., 2022).
147 In undamaged wing discs, cells in S-phase were distributed evenly throughout the wing
148 disc (Fig. 1B). However, after tissue damage, the blastema had increased EdU
149 incorporation (Fig. 1C,D), suggesting more cells were in S phase. Similarly, mitotic cells
150 appeared uniform throughout an undamaged wing disc (Fig. 1E), but the regeneration
151 blastema had an increased number of mitotic cells (Fig. 1E,F,G).
152
153 Next, we asked if regeneration also involves increased growth driven by protein
154 translation. To examine protein translation, we used the O-propargyl-puromycin (OPP)
155 assay, which marks newly synthesized protein by incorporating a puromycin analog
156 detected by click chemistry. In undamaged discs, translation seemed evenly distributed
157 throughout (Fig. 1H). However, after tissue damage, the blastema had markedly
158 increased translation (Fig. 1I,J).
159
160 Given that proliferation and translation were elevated in the regeneration blastema, we
161 asked what drives this robust growth. To answer this question, we examined Ecdysone
162 Receptor (EcR) activity, glycolysis, Myc expression, and Tor signaling. We first asked

whether blastema cells escape reduced growth caused by reduced ecdysone by upregulating activity of the EcR (Fig. S1). Indeed, our transcriptional profile of the regeneration blastema showed slight upregulation of *EcR*, a log2 increase of 1.16 (p=0.00005)(Khan et al., 2017). In addition, EcR activity is increased during later regeneration (R32) and is important for regeneration (Terry et al., 2024). To assess EcR activity at R24 we used the *7xEcRE-GFP* reporter, which has seven EcR response elements (EcREs) upstream of GFP (Hackney et al., 2007; Terry et al., 2024). The EcRE-GFP reporter was active throughout an undamaged wing pouch (Fig. S1C) and was not elevated in the blastema at R24 (Fig. S1D), indicating that enhanced EcR activity does not drive growth at R24.

Glycolysis is increased during early zebra fish fin regeneration due to the upregulation of lactate dehydrogenase (Ldh) (Brandão et al., 2022). Therefore, we asked whether increased glycolysis and lactate dehydrogenase might be driving the growth in the *Drosophila* regeneration blastema. However, a reporter line for *Lactate dehydrogenase* (*Ldh*) expression, *Ldh-GFP*^{Genomic} (Bawa et al., 2020; Rai et al., 2024), did not show increased expression in the blastema (Fig. S1E,F). Thus, upregulated Ldh does not drive the robust growth in the regeneration blastema.

Myc is a transcription factor that regulates cell growth by promoting proliferation and translation (Bellosta and Gallant, 2010; Grewal et al., 2005; Johnston et al., 1999) and is important for regeneration in multiple animals, including Hydra, Axolotl, *Xenopus*, and zebrafish (reviewed in Ascanelli et al., 2024). In *Drosophila* imaginal discs, Myc is highly expressed in the blastema, overexpression of Myc leads to better regeneration, and reduction of Myc causes poor regeneration (Abidi et al., 2023; Harris et al., 2020; Serras and Bellosta, 2024; Smith-Bolton et al., 2009). To determine whether Myc is upregulated through transcription, we used a *Myc-lacZ* reporter line. In undamaged discs, *Myc-lacZ* expression was observed throughout the pouch, with a slight reduction at the dorsal-ventral boundary (Fig. 1K). At R24, *Myc-lacZ* was upregulated in the regeneration blastema (Fig. 1L-M). We previously found that Myc expression was difficult to reduce

during regeneration, either through RNAi knockdown or use of a heterozygous mutation (Abidi et al., 2023), suggesting that its expression is tightly regulated.

Tor regulates translation by phosphorylating ribosomal p70 S6 kinase I (S6K), which in turn phosphorylates ribosomal protein S6 (RpS6) (reviewed in Frappaolo and Giansanti, 2023). We examined Tor pathway activity through anti-phospho-RpS6 (p-S6) immunostaining (Romero-Pozuelo et al., 2017). In an undamaged wing disc, elevated p-S6 occurred in a patchy pattern (Fig. 1N), consistent with previous studies (Romero-Pozuelo et al., 2017). At R24, p-S6 was enhanced in the regenerating blastema (Fig. 1O-P), suggesting that the Tor pathway might also be an important driver of growth during wing disc regeneration.

Myc promotes regenerative growth in a damaged wing disc

To determine the extent to which Myc contributes to the growth of the blastema, we examined proliferation and protein synthesis in regenerating wing discs with reduced Myc expression. We have previously shown that animals hemizygous for the hypomorphic allele Myc^{P0} substantially reduced Myc throughout the wing disc and eliminated the elevated Myc in the blastema of regenerating wing discs, leading to poor regeneration (Abidi et al., 2023)(Fig. S2A,B). By comparing EdU incorporation in the control and the Myc^{P0} regeneration blastemas (Fig. 2A-B), we found a reduction in EdU when Myc levels were reduced (Fig. 2C). Similarly, measurement of mitoses by anti-PH3 staining showed fewer mitotic cells in the Myc^{P0} blastema (Fig. 2D-F, S2C-D). We used the OPP assay to measure protein translation and found that Myc^{P0} regenerating discs had reduced translation (Fig. 2G-I). Thus, Myc promotes growth in the regeneration blastema by promoting translation as well as proliferation.

As Myc regulates growth and translation at least partially through ribosomal biogenesis (Grewal et al., 2005), we examined ribosomal biogenesis by measuring the size of the nucleoli using an anti-Fibrillarin antibody. We measured 10 nucleoli in a 200-pixel^2 area in the hinge and pouch or blastema of each disc. In undamaged discs, the pouch nucleoli and the hinge nucleoli were similar in size (Fig. 2J-L,V). In regenerating wing discs, the

224 blastema cells had larger nucleoli than the hinge cells (Fig. 2M-O,V). Importantly, the
225 nucleoli in the blastema cells were also larger than those in undamaged discs (Fig.
226 2K,N,V).
227
228 To determine whether the nucleoli in the blastema were larger due to increased Myc
229 expression, we measured nucleoli in undamaged and damaged *Myc*^{P0} discs. In *Myc*^{P0}
230 undamaged discs, the nucleoli were the same size in the wing pouch and in the hinge
231 (Fig. 2P-R,V) and smaller than those in control undamaged discs (Fig. 2V). This result
232 was expected because Myc expression was reduced throughout the disc. In *Myc*^{P0}
233 regenerating discs, nucleoli in the *Myc*^{P0} blastema were still larger than the nucleoli in the
234 *Myc*^{P0} hinge (Fig. 2S-U,V) but were smaller than those in the control blastema (Fig.
235 2N,T,V). Therefore, Myc contributes to the increase in nucleolus size in the regeneration
236 blastema but does not account for all of the increase in ribosomal production and
237 nucleolus size.
238
239 **Tor promotes growth in the regeneration blastema**
240 To determine the extent to which Tor signaling contributes to regeneration, we reduced
241 Tor activity using animals heterozygous for *Tor*^{2L1}, a hypomorphic allele that has impaired
242 kinase activity due to a single amino acid change in the kinase domain (Oldham et al.,
243 2000). To confirm that Tor activity was reduced in *Tor*^{2L1}/+ regenerating discs, we
244 assessed anti-p-S6 immunostaining at R24 (Fig. 3A-B), using Wg as a blastema marker
245 (Fig. S3A-B). As expected, p-S6 signal was reduced in *Tor*^{2L1}/+ regenerating discs (Figs.
246 3A-C, S3A-B). In addition, we examined the adult wings that developed from regenerated
247 discs of *Tor*^{2L1}/+ flies as a proxy for how well regeneration occurred in the imaginal disc.
248 The *Tor*^{2L1}/+ flies had smaller wings after disc regeneration, indicating that the imaginal
249 discs had regenerated poorly (Fig. S3C).
250
251 We assessed proliferation in *Tor*^{2L1}/+ regenerating discs using EdU incorporation and
252 anti-PH3 staining (Figs. 3D-I, S3D-E). EdU intensity was reduced when Tor activity was
253 reduced (Fig. 3D-F). Similarly, the number of mitotic cells per area was reduced when
254 Tor activity was reduced (Figs. 3G-I, S3D-E).

255

256 We examined protein translation in *Tor*^{2L1}/+ regenerating discs using the OPP assay, and
257 found reduced protein translation in the blastema when Tor signaling was reduced (Figs.
258 3J-L, S3F-G). Thus, we concluded that Tor signaling promotes regeneration blastema
259 growth by regulating both proliferation and translation. Interestingly, we noticed that the
260 area marked by Wg expression was smaller than the area with upregulated translation
261 (Fig. 3J-K), suggesting that regenerative growth may be elevated outside of the zone
262 marked by expression of canonical blastema genes.

263

264 Next, we asked if Tor enhances growth in part by enhancing ribosomal biogenesis.
265 However, the nucleoli in the blastemas of *Tor*^{2L1}/+ discs were not smaller than those in
266 the controls (Fig. S3H-N). We wondered if the heterozygous *Tor*^{2L1} allele was not strong
267 enough for us to detect a requirement for Tor in ribosomal biogenesis. Therefore, we fed
268 the larvae rapamycin to reduce Tor signaling (Fig. 3M-S). While the blastema cells had
269 larger nucleoli than cells in the hinge in both control and rapamycin-fed animals, (Fig.
270 3M,P), the rapamycin-fed animals had smaller nucleoli in the blastema compared to those
271 in larvae fed control food (Fig. 3N,Q,S). Thus, Tor signaling is important for ribosome
272 biogenesis during regeneration.

273

274 **Crosstalk between Tor signaling and Myc in the regeneration blastema**

275 Several studies have shown interactions between Myc and Tor in regulating growth in
276 *Drosophila* (Kuo et al., 2015; Parisi et al., 2011; Teleman et al., 2008). Thus, we asked
277 whether there is also crosstalk between Myc and Tor in the regeneration blastema. First,
278 we asked whether regenerating discs with reduced Myc have reduced Tor activity by
279 immunostaining for p-S6 in *Myc*^{P0}/*Y* regenerating discs and found reduced p-S6 intensity
280 (Fig. 3T-V). Thus, Myc is important for increased Tor signaling in the regeneration
281 blastema.

282

283 Next, we asked if reduced Tor activity would reduce Myc expression in the regeneration
284 blastema. We used rapamycin feeding to inhibit Tor activity and the *Myc-lacZ* reporter to
285 examine Myc transcription. We saw reduced transcription of the Myc reporter in the

animals fed with rapamycin, compared to the animals fed with control food (Fig. 3W-Y), suggesting that Tor signaling regulates Myc expression. Together, these results establish the existence of crosstalk between Myc and Tor signaling in the regeneration blastema.

Mapping the domain of high Myc expression in the regeneration blastema

Two sets of scRNA-seq data from regenerating *Drosophila* wing imaginal discs identified cells belonging to the regeneration blastema: called blastema 1 and blastema 2 cells (Worley et al., 2022), or wound alpha cells (Floc'hlay et al., 2023). The ablation assays used in these two studies were slightly different; we used the pro-apoptotic gene *reaper* to induce cell death whereas these studies used the TNFα *eiger*. In addition, Floc'hlay et al. activated ablation for 40 hours instead of the 24 hours that we and Worley et al. used. Therefore, to confirm that the expression of the blastema markers in our ablation system is similar to those identified in these reports, we used Upd3, a JAK/STAT ligand, as a blastema 1 marker and Wg as a blastema 1 and 2 marker (Worley et al., 2022). To visualize *upd3* expression, we used the reporter line *upd3-lacZ* (Bunker et al., 2015). In regenerating wing discs, we confirmed two zones in the regeneration blastema, in which the Wg-expressing area was larger than the *upd3-lacZ*-expressing area (Fig. 4A-B'), confirming the existence of blastema 1 and 2 cells in our discs. To understand where Myc is upregulated, we used Wg as a blastema marker and co-immunostained for Myc. While Wg did not co-localize with Myc in an undamaged disc (Fig. 4C), in R24 discs, high Myc expression coincided with high Wg expression as previously reported (Smith-Bolton et al., 2009)(Fig. 4D-D').

We also determined the extent to which the blastema as defined by Worley et al. coincided with Nubbin (Nub) expression, which is normally found in the wing pouch and overlaps with the inner ring of Wg at the boundary between the pouch and the hinge (Ng et al., 1995; Terriente et al., 2008). In an undamaged wing disc, the Nub-expressing area was slightly larger than the moderate Myc-expressing area (Fig. 4E). During regeneration, the Nub-expressing area was also larger than the high Myc-expressing area (Fig. 4F-F'). Therefore, the blastema as defined by Wg and Myc expression is smaller than the Nub-expressing area. To determine which cells in the regenerating disc were hinge cells and

317 if there is any overlap between the hinge and the regeneration blastema, we used a Zfh2
318 antibody (Tran et al., 2010) (Fig. 4G-H') and the JAK/STAT signaling reporter
319 *10XSTAT92E-GFP* (Bach et al., 2007) (Fig. 4I-J') as hinge markers. In both undamaged
320 (Fig. 4G,I) and damaged discs (Fig. 4H-H',J-J'), the hinge markers were expressed
321 directly adjacent to, but not overlapping with, the zone with elevated Myc expression.
322
323 To ask whether Nub and Zfh2 expression overlapped in regenerating discs, we used the
324 *nub-MiMIC-GFP* (*nub*^{MI05126}) line, in which a MiMIC transposable element inserted into
325 the *nub* locus expresses GFP in cells that are also marked with anti-Nub immunostaining
326 (Khan et al., 2017; Venken et al., 2011b). In undamaged wing discs, Nub-GFP expression
327 overlapped with Zfh2-positive cells at the inner ring of Wg expression (Fig. 4K), consistent
328 with previous studies (Terriente et al., 2008). In regenerating wing discs, we also found
329 Nub-GFP expression overlapping with Zfh2 expression (Fig. 4L, S4). Furthermore, Wg,
330 Nub, and Zfh2 expression together showed that the blastema was smaller than the Nub-
331 expressing area but directly adjacent to the cells expressing both Nub and the hinge
332 markers (Fig. 4L,L"). Interestingly, hinge cells adjacent to the blastema are flexible in their
333 identity and can become pouch cells during re-growth (Herrera et al., 2013; Ledruet al.,
334 2022; Worley et al., 2018), which may be occurring in the cells expressing both Nub and
335 Zfh2. Thus, the high Myc-expressing zone colocalized with the blastema as defined by
336 single-cell sequencing and did not overlap with hinge cells.
337
338 **The regeneration blastema includes additional zones of elevated growth outside**
339 **the canonical blastema**
340 While immunostaining for p-S6, we marked the blastema by immunostaining for Wg and
341 found that the region with elevated Tor activity was larger than the area with Wg
342 expression (Fig. 3A). In addition, the region marked with the OPP translation assay was
343 also larger than the Wg-expressing area (Fig. 3J'). Thus, we sought to better understand
344 the spatial relationships among the blastema, Myc expression, Tor signaling, and
345 enhanced translation. Given that anti-Myc and anti-p-S6 are both rabbit antibodies, and
346 that Myc and Wg expression co-localized, we used the Wg antibody to mark the Myc-
347 expressing blastema cells. By visualizing Wg, p-S6, and translation, we discovered

348 additional concentric zones of the regeneration blastema. Wg, marking the canonical
349 blastema, was expressed in the center, which we call Growth Zone A (Fig. 5A,B), and
350 which also had elevated p-S6 and OPP signal (Fig. 5C,D). Growth Zone B, the area
351 outside of Zone A, had high p-S6 but not Wg (Fig. 5A,C-E). Growth Zone C was the area
352 with high translation but not upregulated Wg, Myc, or p-S6 (Fig. 5A,F-G). To confirm the
353 existence of these zones, we quantified the area of each (Fig. 5H,I) and examined the
354 fluorescence intensity profile of a cross-section through the wing disc (Fig. S5A-G'). Both
355 analyses indicated that there were three distinct zones within the regeneration blastema.
356
357 We wondered whether the OPP signal in Zone C that extended beyond Zone B was
358 caused by Tor signaling non-autonomously inducing increased translation, or by spread
359 of the OPP signal, or by an unknown additional factor that increases translation. To test
360 the extent to which Tor activity can induce OPP signal non-autonomously, we activated
361 Tor in the posterior half of an undamaged wing disc using *hhGal4, UAS-Tsc2RNAi*
362 (*hh>Tsc2i*) and performed the OPP assay and p-S6 immunostaining (Fig. S5H-Q). The
363 elevated OPP signal extended beyond the A/P boundary while the p-S6 immunostaining
364 did not (Fig. S5H-Q). Therefore, either Tor activity can induce elevated translation in the
365 adjacent cells or the OPP assay signal can spread, perhaps due to newly synthesized
366 secreted or extracellular proteins labeled with OPP.
367
368 To determine whether Growth Zone C coincided with the Nub-expressing area, we
369 combined the OPP assay with Nub immunostaining (Fig. 5J-L). The Nub+ area was
370 slightly larger than the area with elevated translation, indicating that Growth Zone C is
371 smaller than the remaining inner hinge (Fig. 5J-L).
372
373 **The concentric growth zones have different proliferation rates**
374 We wondered whether these blastema zones were biologically relevant. Therefore, we
375 asked if cell proliferation was different across these zones. Given that anti-PH3 and anti-
376 p-S6 are both rabbit antibodies, we could not use p-S6 to mark Zone B. Therefore, we
377 took an approximate approach by measuring the area of each zone and calculating the
378 average radius. We used the radii to determine the distances between the edges of

379 Growth Zones A, B, and C. Using these measurements, the average distance between
380 the edges of Growth Zone A and B was 13 microns, and the average distance between
381 the edges of Growth Zone B and C was 16 microns (Fig. 5A,I). We then immunostained
382 for Wg to establish the boundary of Growth Zone A, and measured concentric zones
383 based on the shape of Wg immunostaining (Fig. 5M). We then assessed mitoses per area
384 in each zone (Fig. 5N). Proliferation was highest in Growth Zone A, was slightly reduced
385 in Growth Zone B, and was lower still in Growth Zone C. Proliferation in the cells 10
386 microns outside of Growth Zone C was even lower. Thus, these growth zones are
387 biologically meaningful and likely contribute at different levels to regenerative growth.
388
389 **Differences in Myc expression induce cell death at the periphery of Growth Zone A**
390 Given the difference in Myc levels between Growth Zone A and the rest of the disc, we
391 wondered whether cell competition was occurring. We quantitated cell death using the
392 terminal d-UTP nick-end labeling (TUNEL) assay. Since we used apoptosis to induce
393 tissue damage, we needed to distinguish between ablation and cell competition. We used
394 *UAS-eGFP* to mark apoptotic cells eliminated by our ablation system. At R0, GFP-
395 expressing debris was found on both the basal and the apical sides of the epithelium (Fig.
396 6A). However, at R24, the GFP-containing debris on the basal side of the epithelium was
397 mostly gone (Fig. 6B), and most of the TUNEL-positive cells did not express GFP (Fig.
398 6B).
399
400 Cells undergoing apoptosis due to cell competition are extruded toward the basal side of
401 the epithelium (Amoyel and Bach, 2014; Li and Baker, 2007). In addition, cell death driven
402 by Myc-induced super-competition occurs within an eight-cell zone adjacent to the winner
403 cells (De La Cova et al., 2004). Thus, we counted TUNEL+ cells on the basal side of the
404 epithelium in an 8-cell zone. To set a baseline for quantification, we quantified TUNEL in
405 a negative control, in which *dpp-Gal4* was used to drive *UAS-GFP* in a normally
406 developing wing disc, and a positive control, in which *dpp-Gal4* was used to drive *UAS-*
407 *Myc*. In the negative control, there were no Myc expression differences and no TUNEL-
408 positive cells (Fig. 6C,C',G). In the positive control, cell death was observed in cells
409 located inside the high-Myc stripe and in cells located within an eight-cell region adjacent

410 to the high-Myc cells (Fig. 6D,D',G). These results concurred with previous studies (De
411 La Cova et al., 2004).
412
413 We then quantified TUNEL-positive cells in regenerating discs that were on the basal side
414 of the epithelium within an eight-cell-wide band outside of the Myc-expressing cells, which
415 measured about 39 μm (Fig. 6E,E',H). We found that the number of TUNEL-positive cells
416 in this eight-cell band was even higher than in the positive controls (Fig. 6E-E',G). We
417 examined cell death at 48 hours and 72 hours after tissue damage and found that the cell
418 death continued throughout regeneration (Fig. S6A-C). To determine whether this
419 apoptosis was due to elevated Myc expression, we quantified TUNEL-positive cells in
420 *Myc*^{P0} regenerating discs (Fig. 6F,F',G). Surprisingly, the overall number of TUNEL-
421 positive cells on the basal side of the epithelium was not reduced in *Myc*^{P0} regenerating
422 discs (Fig. 6G). However, the number of TUNEL-positive cells inside of the Wg+ zone in
423 *Myc*^{P0} discs was higher (Fig. 6H,I), and cell death at the periphery of the Wg+ zone was
424 significantly reduced (Fig. 6H,J). This finding suggests that the cell death observed
425 outside of the Wg+ and Myc+ zone is due to Myc expression level differences. The
426 increased cell death within the Wg+ zone in *Myc*^{P0} regenerating discs suggests that Myc
427 is important for survival of these blastema cells. The blastema is subject to complex
428 signaling interactions due to the damage response, which may lead to this requirement
429 for elevated Myc for cell survival.
430
431 **Cell competition induced in regenerating wing discs is distinct from experimentally**
432 **induced cell competition**
433 Cell competition and super-competition studies usually involve genetic clones that differ
434 by one or two factors relative to the surrounding cells, experimentally establishing a
435 mismatch in cell fitness. However, in regenerating imaginal discs, there are overlapping
436 and adjacent zones of elevated Wg, JAK/STAT, Yki, JNK, p38, and Tor signaling
437 (Bergantiños et al., 2010; Grusche et al., 2011; Santabárbara-Ruiz et al., 2015; Smith-
438 Bolton et al., 2009; Sun and Irvine, 2011) (Figs. 4C-D',I-J', 5B,E), which may render
439 fitness comparisons during regeneration more complex than the binary comparisons
440 made in cell competition studies. Therefore, to ask whether the cells outside the high Myc

zone were behaving like “loser cells”, we examined three different factors that are important for loser cell fate in cell competition and super-competition, proteotoxic stress, autophagy, and expression of Xrp1.

The distinction between cell competition and super-competition is based on whether wild-type cells are winner cells or loser cells (Morata, 2021). However, it is unclear whether the cells outside of the high-Myc zone in regenerating discs can be described as wild-type cells because Myc levels are lower than in normal discs. In addition, Myc levels in the blastema are elevated relative to the rest of the disc and relative to undamaged discs but are not as high as when Myc is overexpressed. Given that loser cells during cell competition have increased eIF2α phosphorylation (Baumgartner et al., 2021; Kiparaki et al., 2022), and winner cells during super-competition also have increased eIF2α phosphorylation (Paul et al., 2024), we examined phospho-eIF2α levels in regenerating discs to determine which type of cell competition was occurring.

In an undamaged wing disc, eIF2α was phosphorylated throughout the disc (Fig. 7A). After tissue damage, phosphorylation of eIF2α was reduced in the Wg+ zone of the regeneration blastema, which are the “winner” cells (Fig. 7B-B’). Therefore, the enhanced translation in the blastema did not cause proteotoxic stress, and the regenerating disc may be experiencing something closer to cell competition and not super-competition.

Cell elimination due to cell competition can involve an increase in autophagy (Nagata et al., 2019). Therefore, we used the autophagy marker *Atg8a-mcherry* (Hegedűs et al., 2016; Mauvezin et al., 2014) and counted mCherry-positive puncta in the cells directly adjacent to the Wg+ zone (the boundary) and in the cells within the eight-cell perimeter outside of the Wg+ zone (Fig. 7C-E, S6D-E). While there were few or no mCherry-positive puncta in undamaged wing discs (Fig. 7C, S6D), mCherry-positive puncta were observed in regenerating wing discs (Fig. 7D, S6E), particularly at the boundary and in the cells within the 8-cell perimeter outside of the Wg+ zone (Fig. 7E).

471 Xrp1 is a basic leucine zipper domain (bZIP) protein that is expressed in loser cells and
472 is essential for loser cell elimination during imaginal disc cell competition (Baillon et al.,
473 2018; Kiparaki et al., 2022; Lee et al., 2018; Ochi et al., 2021). We did not detect
474 expression level differences between the cells inside the blastema and the cells
475 surrounding the blastema using an Xrp1 antibody (Brown et al., 2021) (Fig. 7F-G) an
476 *Xrp1-GFP* in which the Xrp1 protein is tagged with GFP (Fig. S6F-F")(Kudron et al., 2018),
477 or an enhancer trap line *Xrp1-lacZ*^{02515} (Bellen et al., 2004) (Fig. 7H-I). Therefore, the cell
478 death surrounding the high Myc area in the blastema might not be mediated through *Xrp1*.
479
480 To confirm that cell death surrounding the high-Myc area is not mediated by *Xrp1*, we
481 examined cell death in regenerating wing discs that were heterozygous for the mutant
482 *Xrp1*$^{m2-73}$, which is a truncated allele that eliminates cell competition when heterozygous
483 (Lee et al., 2016; Lee et al., 2018). Cell death surrounding the Wg+ blastema zone was
484 not reduced in *Xrp1*$^{m2-73}$/+ discs (Fig. 7J-K, S6G-H). Given that Xrp1 is not differentially
485 expressed, and that heterozygous *Xrp1* does not rescue the cell death at the periphery
486 of the blastema, it is unlikely that Xrp-1 mediates this Myc-induced cell death.
487
488 Several mechanisms can mediate the fitness comparison in traditional cell competition,
489 including expression of the loser isoforms of *flower* (*fwe*), *fwe*^{loseA} and *fwe*^{loseB}, and *azot*
490 in the loser cells (Merino et al., 2015; Rhiner et al., 2010), and expression of the Spatzle-
491 processing enzymes SPE or ModSP in the winner cells to activate Spatzle and induce
492 Toll signaling in loser cells (Alpar et al., 2018; Germani et al., 2018; Meyer et al., 2014).
493 We did not find an increase in *fwe*^{loseA}, *fwe*^{loseB}, or *azot* expression in regenerating wing
494 discs in the low-Myc cells (Fig. S7A-C', R-S). We also did not find a reduction in cell death
495 in discs heterozygous for an *azot* mutant (Fig. S7D, R-S), and we found a global reduction
496 in cell death in discs heterozygous mutant for the entire *fwe* locus (Fig. S7E, R-S).
497
498 While SPE can be upregulated in winner cells, our published transcriptional profile
499 suggested that *SPE* is downregulated in the blastema with a log2 decrease of 1.57
500 (p=0.00005)(Khan et al., 2017). Furthermore, whole-disc RT-qPCR showed no difference
501 in *SPE* expression after damage (Fig. S7F). We used in situ hybridization chain reaction

502 (HCR) to examine the spatial distribution of *SPE* mRNA (Fig. S7G) (Choi et al., 2018; S
503 Bruce et al., 2021). *SPE* mRNA was not different between Growth Zone A and the
504 adjacent 8-cell band (Fig. S7H). *modSP* mRNA levels were not elevated in our
505 transcriptional profile (Khan et al., 2017). We examined spatial expression of *modSP* by
506 HCR, which was upregulated in experimentally induced winner cells in an undamaged
507 disc but was not upregulated in Zone A of a regenerating disc (Fig. S7I-K). To assess
508 activation of Toll signaling, we quantified the amount of Dorsal immunostaining present
509 in the nuclei of cells inside and outside Zone A (Fig. S7L). Given that the antibodies
510 against Dorsal and Wg were both generated in mice, Zone A was marked by a newly
511 generated transgenic line, *2xHA-Myc*, in which a 2xHA-tag was added to the N terminus
512 of the endogenous *Myc* gene (Fig. S7L'). While some Dorsal translocated into the nucleus
513 inside of the Zone A cells (Fig. S7M-N,O), its location remained cytoplasmic in the cells
514 outside of Zone A (Fig. S7M'-N',O). To ask whether SPE is required for death in the 8-
515 cell zone, we quantified TUNEL in regenerating discs heterozygous for the SPE^{SK6}
516 mutation (Fig. S7P,R,S) or expressing *UAS-SPE-RNAi* (Fig. S7Q,T,U). We did not find
517 reduction of cell death surrounding the high-Myc area in either condition.
518
519 Taken together, these data suggest that increased Myc in the regeneration blastema
520 leads to something closer to cell competition than super-competition, given the absence
521 of cell death when Myc levels were equalized, the increased proteotoxic stress, and the
522 presence of autophagy. Additionally, Myc-induced cell death outside the high-Myc zone
523 is not identical to canonical cell competition, which is mediated by Xrp1 and can involve
524 Azot expression or Toll signaling activation. Therefore, we conclude that the cell death
525 seen around the Wg+, high-Myc Zone A does not fall neatly into the types of cell
526 competition characterized through experimentally induced clones.
527
528
529 **Discussion**
530 We have shown that Myc and Tor are two critical factors that regulate regenerative growth.
531 Reduction of either Myc expression or Tor kinase activity impaired proliferation and
532 translation in the regeneration blastema. Furthermore, our findings revealed concentric

533 growth zones that extend beyond the blastema as defined by transcriptional profiling. We
534 also demonstrated that the upregulated Myc expression induces cell competition-like cell
535 death in the surrounding cells.
536
537 In our concentric growth zone model, the growth zones were differentiated through
538 expression of genes such as Wg and Myc, activated Tor signaling, and elevated
539 translation. Given that the shape of each zone is similar, it is likely that some secreted
540 factor in Growth Zone A establishes the outer zones, perhaps through damage-response
541 signaling such as reactive oxygen species, morphogen signaling such as Wg, or
542 mechanical signaling such as the Hippo pathway. Furthermore, the high translation in
543 Zone C may be a non-autonomous effect of high Tor activity in Zone B. Interestingly,
544 these distinct zones were not identified by scRNA-seq experiments (Floc'hlay et al., 2023;
545 Worley et al., 2022), suggesting that the cells in Zones B and C may not have differential
546 gene expression. However, these studies induced damage through overexpression of
547 Eiger, whereas we induced damage through overexpression of Reaper, and the blastema
548 after Eiger-induced ablation may not have different zones of Myc expression and Tor
549 activity.
550
551 Evidence for a similar gradient in proliferation has been observed in other regeneration
552 models. For example, in zebrafish fin regeneration, differential expression of *msxb*, a
553 homeodomain transcriptional repressor, gives rise to a proliferation gradient that occurs
554 between the proximal and distal blastema (Nechiporuk and Keating, 2002). In addition,
555 mTor signaling is also essential for zebrafish fin regeneration (Hirose et al., 2014; Xiao et
556 al., 2024) and axolotl limb regeneration (Zhulyn et al., 2023). Thus, transcription factors
557 and Tor signaling may establish zones of regenerative growth in many systems.
558
559 The enhanced Myc expression in the regeneration blastema has a double-edged effect
560 on the regenerating wing disc. While Myc drives regrowth in Growth Zone A, it also
561 induces cell death in the neighboring cells, which include Growth Zones B and C,
562 tempering their ability to contribute to the regenerated tissue. Although this cell death was
563 mediated by Myc, with proteotoxic stress and autophagy increased in the loser cells, the

loser cells did not upregulate Xrp1, Azot expression, or Toll signaling. Thus, these interactions did not completely resemble cell competition as described in previous studies. Notably, while Growth Zone A cells had high Myc expression and thus were winner cells, the cells outside of Growth Zone A still had elevated translation. In addition, JAK/STAT signaling was also high outside of growth Zone A, and JAK/STAT signaling can both induce cell competition and rescue loser cell death (Rodrigues et al., 2012). Furthermore, JNK signaling, Yki activity, and mechanical stress can also influence cell competition (Baker, 2020; Morata, 2021). Thus, regeneration occurs in a more complex signaling milieu than classical cell competition experiments and may provide clues to how cell competition operates in other complex microenvironments such as tumors. Furthermore, our work presents the first evidence of endogenous cell competition in a non-stem cell-based regeneration model, further exploration of which will enhance our understanding of both regeneration and cell competition.

Materials and Method

Tissue ablation

Ablation experiments were performed as previously described (Smith-Bolton et al., 2009). Briefly, egg lays were performed at 25°C in the dark for 4 hours, then incubated at 18°C. First-instar larvae were picked on day 2 and placed in vials, 50 larvae/vial. On day 7, vials were incubated for 24 hours in a 30°C circulating water bath, kept on ice for 5 minutes to reduce the temperature, then returned to the 18°C incubator *Myc*^{P0} animals had ablation induced 4 hours later to coincide with the early third instar stage because they have delayed development (Abidi et al., 2023).

Drosophila strains

Fly lines used were: *w*^{1118} (Hazelrigg et al., 1984); *w*^{1118}*; rnGal4*, *UAS-rpr*, *tubGal80ts/TM6B*, *tubGal80* (Smith-Bolton et al., 2009); *7xEcRE-GFP (Hackney et al., 2007; Terry et al., 2024)*(a gift from Kenneth Moberg); *Myc-lacZ* (RRID:BDSC_12247); *Myc*^{P0} (Johnston et al., 1999)(RRID:BDSC_11298); *Tor*^{2L1}(Oldham et al., 2000)(RRID:BDSC_98102); *Upd3-lacZ* (Bunker et al., 2015)(a gift from David Bilder); *10XStat92E-GFP* (Ekas et al., 2006)(RRID:BDSC_26197); Nub-*MiMIC-GFP*

(*Mi{MIC}nub*^{MI05126})(Venken et al., 2011a)(RRID:BDSC_37920); *UAS-Myc* (Johnston et al., 1999)(RRID:BDSC_9674); *UAS-GFP* (Shiga et al., 1996)(RRID:BDSC_4775); *Dpp-Gal4* (Kojima et al., 2000)(RRID:BDSC_93385); *Xrp1-lacZ* (Bellen et al., 2004) (RRID:BDSC_11569); *Xrp1-GFP* (Kudron et al., 2018) (RRID:BDSC_83391), *Xrp1*$^{M2-73}$ (Lee et al., 2018)(RRID:BDSC_81270); *3xmCherry-Atg8a (Hegedűs et al., 2016)*(a gift from Juhász Gábor); *fwe*^{loseA}*::mcherry KI* (Levayer et al., 2015), *fwe*^{loseB}*::mcherry KI , azot{KO; gfp} (Merino et al., 2015)*(gifts from Christa Rhiner); *fwe*^{DB56}(RRID:BDSC_51610); *SPE*^{SK6} (Yamamoto-Hino et al., 2015); *UAS-SPE-RNAi* (RRID:BDSC_33926); *2xHA-Myc* (this paper).

Generation of 2xHA-Myc transgenic line

To generate an HA-Myc transgenic fly line, we used the Scarless Gene Editing technique (Gratz et al., 2024). Homology arms 1kb upstream of the Myc transcription start site and 1kb downstream of the Myc transcription start site were cloned into the pHD-2xHA-ScarlessDsRed plasmid (DGRC Stock 1366; RRID:DGRC_1366), flanking the 2xHA and the DsRed cassette (cloning performed by Genscript). The gRNA sequence (ttcagACAGGCATATAACTCAG) was cloned into the pCFD5 plasmid at the BbsI site. These plasmids were injected into PBac{y[+mDint2] GFP[E.3xP3]=vas-Cas9}VK00027 (RRID:BDSC_51324). Injection services were provided by Bestgene. We crossed the 2xHA-DsRed-Myc fly lines to a piggyBac transposase line (RRID:BDSC_8285) to remove the DsRed marker.

Immunostaining

Immunostaining was carried out as previously described (Smith-Bolton et al., 2009). After dissection, the larval carcasses were fixed in 4% paraformaldehyde (PFA) for 20 minutes at room temperature, followed by 3 washes in 0.1% triton in phosphate-buffered saline (PBS) (0.1% PBST) for 10 minutes. Carcasses were incubated at 4°C overnight in primary antibodies diluted as noted below in 10% normal goat serum and 0.1% PBST, followed by 3 washes of 0.1% PBST for 10 minutes. Secondary antibody was diluted 1:1000 in 10% normal goat serum and 0.1% PBST for incubation at 4°C overnight. After the secondary

626 antibody incubation, the samples were washed 3 times using 0.1% PBST, followed by
627 incubation in 70% glycerol in PBS overnight at 4°C. The wing imaginal discs were then
628 dissected and mounted on slides with Vectashield Anti-fade mounting media (Vector
629 Laboratories, Cat #H-1000).
630
631 Primary antibodies used: anti-Myc (1:250, Santa Cruz Biotechnologies, #sc-28207), anti-
632 p-S6 (Romero-Pozuelo et al., 2017) (1:200, a gift from Aurelio Teleman), anti-phospho-
633 Histone H3 (1:500, Millipore Sigma, #06-570), anti-Nubbin (RRID:AB_2722119) (1:250,
634 Developmental Studies Hybridoma Bank (DSHB), #Nub2D4), anti-Wingless
635 (RRID:AB_528512) (1:100, DSHB, #4D4), anti-Zfh2 (Tran et al., 2010) (1:250, a gift from
636 Chris Doe), anti-β-Galactosidase (1:500, Invitrogen, Thermo Fisher Scientific #A-11132),
637 anti-p-eIF2α (1:100, Cell Signaling, #3398), anti-Xrp1 (Brown et al., 2021) (1:1000, a gift
638 from Hyung Don Ryoo), anti-Fibrillarin (1:100, Abcam, #ab4566), anti-Dorsal (1:20, DSHB,
639 7A4), anti-HA (1:1000, Cell Signaling, #3274). Secondary antibodies were Alexa Fluor
640 488, 555, 633, 647 (1:1000, Invitrogen) and DAPI (1:1000, Thermo Fisher Scientific
641 #D1306).
642
643 ***In Situ* Hybridization Chain Reaction (HCR)**
644 The HCR technique was carried out using the HCR Gold RNA-FISH kit (Molecular
645 Instrument) as previously described (Choi et al., 2018; S Bruce et al., 2021) with some
646 modifications. After dissection, the larval carcasses were fixed in 4% paraformaldehyde
647 (PFA) for 20 minutes at room temperature, followed by 3 washes in 0.1% triton in
648 phosphate-buffered saline (PBS) (0.1% PBST) for 10 minutes. After the washes, the
649 samples were incubated in pre-hybridization buffer at 37°C for 30 minutes, followed by
650 incubation with probes at 37°C for 2 nights. Probe washing and amplification steps were
651 conducted as described (S Bruce et al., 2021). DAPI (1:1000) was added during the
652 hairpin incubation step. Probes used: SPE (3:200), ModSP (3:200) (Molecular
653 Instrument).
654
655 **OPP assay**

656 The OPP assay was conducted as described (Kiparaki and Baker, 2023), using the Click-
657 iT Plus OPP Alexa Fluor 488 Protein Synthesis Assay Kit (Thermo Fisher Scientific,
658 #10456). Briefly, larvae were dissected in Schneider's *Drosophila* Medium (Thermo
659 Fisher Scientific, Cat #21720024) with 10% heat-inactivated fetal bovine serum (Thermo
660 Fisher Scientific, Cat #A3840001). Larval carcasses were incubated with component A at
661 the concentration of 10 μM in Schneider's *Drosophila* Medium with 10% heat-inactivated
662 fetal bovine serum for 15 minutes. After rinsing with PBS, the carcasses were fixed in 4%
663 PFA for 20 minutes, followed by 3 washes for 10 minutes each with 0.1% PBST. After
664 washing, carcasses were blocked in 3% bovine serum albumin (BSA) in PBS for 10
665 minutes before the 30 minutes incubation in the cocktail solution for the click-on reaction.
666 After the reaction, samples were washed with the rinse buffer followed by 2 minutes of
667 blocking in 3% BSA in PBS. Protocols after this step followed the general primary and
668 secondary staining method above.
669
670 **EdU incorporation and detection**
671 EdU incorporation and detection was carried out as previously described (Gouge and
672 T.W. Christensen, 2010) using the Click-iT EdU kit (Invitrogen, #C10338). Briefly, larvae
673 were dissected in PBS and incubated in EdU at the concentration of 100 μM in
674 Schneider's *Drosophila* Medium for 30 minutes at room temperature, followed by fixation
675 in 4% PFA for 20 minutes, followed by 3 washes of 10 minutes each with 0.1% PBST.
676 After washing, carcasses were blocked in 3% BSA in PBS for 30 minutes before the 30-
677 minute incubation in the cocktail solution for the click-on reaction. Protocols after this step
678 followed the general primary and secondary staining method above.
679
680 **TUNEL assay**
681 The TUNEL assay was carried out using the *In Situ* Cell Death Detection Kit (Roche,
682 #12156792910). For experiments incorporating the TUNEL assay, we followed the
683 general immunostaining protocol described above. However, for the secondary antibody
684 solution, we used the TUNEL reaction mixture made by mixing the Enzyme Solution and
685 Label Solution at a 1:9 ratio. Secondary antibodies and DAPI were added according to

686 the dilutions listed above. Samples were incubated in this mixture at 4°C overnight,
687 followed by the remainder of the protocol for general immunostaining.
688
689 **Rapamycin food**
690 Rapamycin (Thermo Fisher Scientific, #AAJ62473MC) was dissolved in ethanol at a 50
691 mM concentration. The rapamycin solution was added to Nutri-Fly Bloomington food
692 (Genesee Scientific #66-121) to make a 20μM working concentration. For control food,
693 the same amount of ethanol was added. Immediately after the temperature shift in the
694 circulating water bath, larvae were transferred to rapamycin food or control food.
695
696 **qPCR**
697 qPCR was carried out as previously described (Abidi et al., 2023; Bose et al., 2025).
698 Briefly, 40-50 wing imaginal discs were collected in Schneider's medium (Sigma-Aldrich,
699 #S1046), followed by RNA extraction using the RNeasy Kit (QIAGEN, #74104). cDNA
700 synthesis was done using the SuperScript III First Strand Synthesis Kit (Thermo Fisher
701 Scientific, #11752-050). qPCR reactions were carried out using Power SYBR Green
702 MasterMix (Thermo Fisher Scientific, #A25742) on an ABI StepOnePlus Real-Time PCR
703 System.
704 *Gapdh2* forward primer (GTGAAGCTGATCTCTTGGTACGAC)
705 *Gapdh2* reverse primer (CCGCGCCCTAATCTTTAACTTTTAC) (Classen et al., 2009)
706 SPE forward primer (ACCAATACGACCCTCTGGGA)
707 SPE reverse primer (GCAGTCAGGATCGGTACGAG) (Alpar et al., 2018)
708
709 **Image acquisition**
710 Discs were imaged on a Zeiss LSM 700, Zeiss LSM 880, or Zeiss LSM 900 confocal
711 microscope. All images for a given experiment were acquired on the same microscope
712 with the same instrument settings. Images were processed using ImageJ (NIH).
713 Maximum intensity projections were created for the confocal images. If not otherwise
714 mentioned, the area used for quantification of fluorescence was determined by co-
715 staining for Wg as a Zone A marker (yellow dotted lines). The areas used for quantification
716 for the EdU assay and the *Myc-lacZ* experiments were determined by morphology. The

areas used for quantification of Dorsal in the nucleus was determined by expression of 2xHA-Myc. Within the area expressing 2xHA-Myc, DAPI staining was used to select five nuclei per disc.

Nucleolus measurements

10 nucleoli (anti-Fibrillarin staining) were measured in a 200-pixel x 200-pixel square using ImageJ.

Intensity plots

Intensity plots were made using ImageJ. Briefly, a line across the area of interest was selected using the line selection tool, then an intensity plot was generated using the Plot Profile tool.

Statistical analysis

All statistical analyses were performed using Welch's t-test on Graphpad Prism. Graphs were made on Graphpad Prism.

Acknowledgments

The authors would like to thank Anish Bose, Snigdha Mathure, and Connor Powers for critical reading of the manuscript and helpful discussions. We thank Dr. Kenneth Moberg, Dr. David Bilder, Dr. Chris Doe, Dr. Hyung Don Ryoo, Dr. Aurelio Teleman, Dr. Juhász Gábor, Dr. Christa Rhiner, and Dr. Satoshi Goto for reagents; the Bloomington Drosophila Stock Center (NIH P40OD018537); the Developmental Studies Hybridoma Bank (NICHD, The University of Iowa); Dr. Glenn Fried, Dr. Duncan Nall, Dr. Umnia Doha, and all the staff at Core Facilities Microscopy suite at the Carl R. Woese Institute for Genomic Biology.

Footnotes

Author contributions

F.T.-Y.H designed, carried out, interpreted the experiments, and prepared the manuscript. R.K.S.-B. designed and interpreted experiments and assisted in preparation of the manuscript.

Funding

This work was supported by the National Institutes of Health grants R01GM107140 and R35GM14174 to R.K.S.-B.

Competing interests

The authors declare no competing or financial interests.

Data and resource availability

All relevant data and resource can be found within the article and its supplementary information. In addition, raw data will be posted in the Illinois Databank (insert URL upon acceptance for publication).

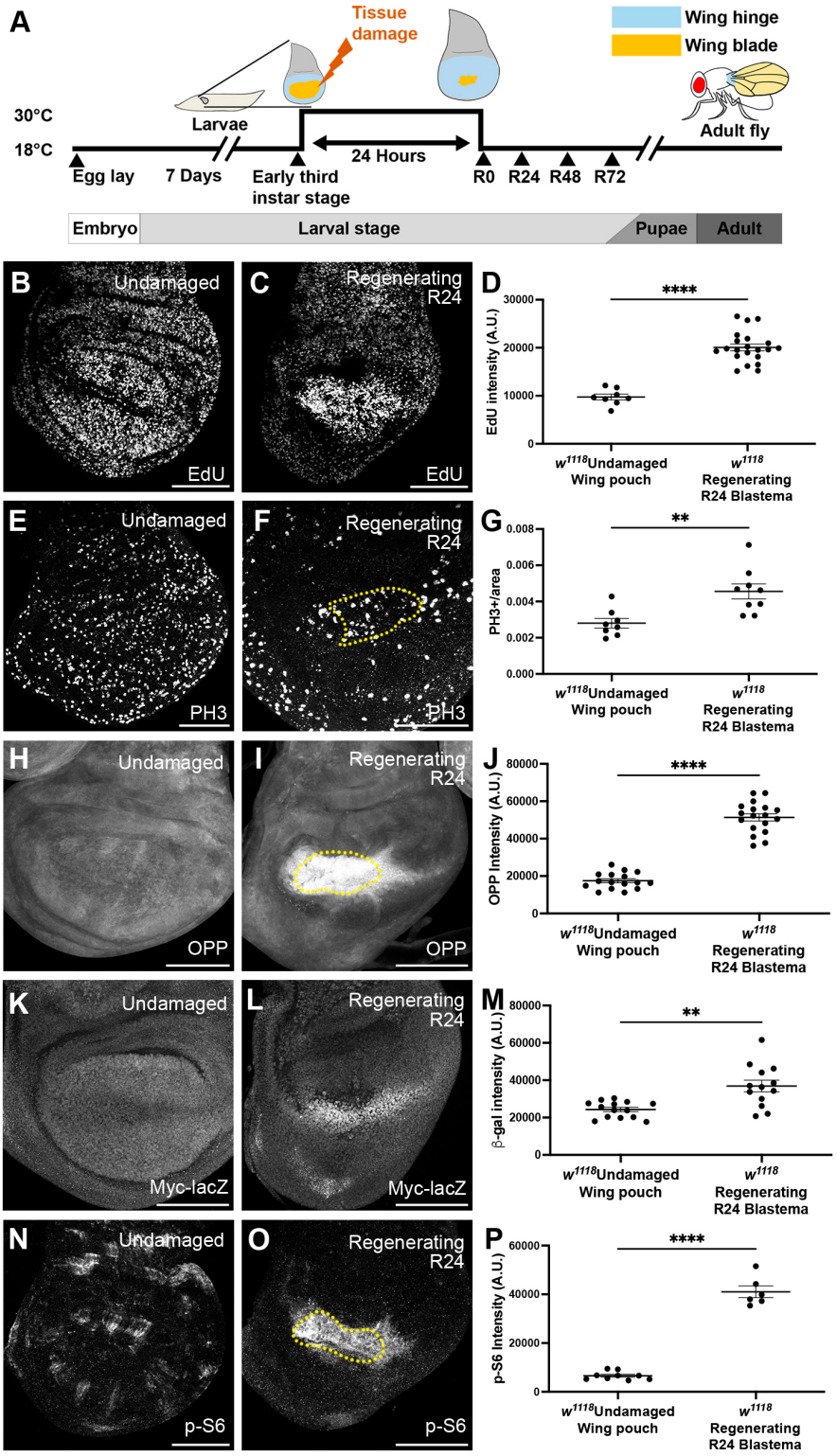
A
Tissue damage
Wing hinge
Wing blade
30°C
18°C
Larvae
Adult fly
24 Hours
Egg lay
7 Days
Early third instar stage
R0
R24
R48
R72
Embryo
Larval stage
Pupae
Adult
B Undamaged EdU
C Regenerating R24 EdU
D
EdU intensity (A.U.)
****
w1118 Undamaged Wing pouch
w1118 Regenerating R24 Blastema
E Undamaged PH3
F Regenerating R24 PH3
G
PH3+/area
**
H Undamaged OPP
I Regenerating R24 OPP
J
OPP intensity (A.U.)
****
K Undamaged Myc-lacZ
L Regenerating R24 Myc-lacZ
M
β-gal intensity (A.U.)
**
N Undamaged p-S6
O Regenerating R24 p-S6
P
p-S6 intensity (A.U.)
****

761 **Figure legends**

762 **Figure 1. Myc expression and Tor signaling in regenerating wing discs**

763 (A) Schematic of the genetic ablation system. (B-C) EdU incorporation marking S-phase
764 cells in an undamaged disc (B) and an R24 disc (C). (D) Quantification of average EdU
765 staining intensity in the wing pouch identified by morphological features. Undamaged
766 n=8, R24 n=21. ****P<0.0001. (E-F) PH3 staining marking mitotic cells in an
767 undamaged disc (E) and an R24 disc (F). (G) Quantification of mitotic cells per area in
768 the wing pouch identified by inner ring of Wg staining (yellow dotted lines in 1F).
769 Undamaged n=8, R24 n=9. **P<0.01. (H-I) OPP assay in an undamaged disc (H) and
770 an R24 disc (I). (J) Quantification of OPP staining intensity in the wing pouch of an
771 undamaged disc or blastema of an R24 disc, identified by the inner ring of Wg staining
772 or Wg staining, respectively. Undamaged n=16, R24 n=18. ****P<0.0001. (K-L) *Myc-*
773 *lacZ* expression detected by β-gal staining in an undamaged disc (K) and an R24 disc
774 (L). (M) Quantification of average β-gal staining intensity in the wing pouch or blastema
775 identified by morphological features. Undamaged n=14, R24 n=13. **P<0.01. (N-O) p-
776 S6 staining in an undamaged disc (N) and an R24 disc (O). (P) Quantification of
777 average p-S6 staining intensity in the wing pouch or blastema identified by Wg staining.
778 Undamaged n=9, R24 n=6. ****P<0.0001. Statistical test used was Welch's t-test. Scale
779 bars are 100μm. Error bars are SEM.

780

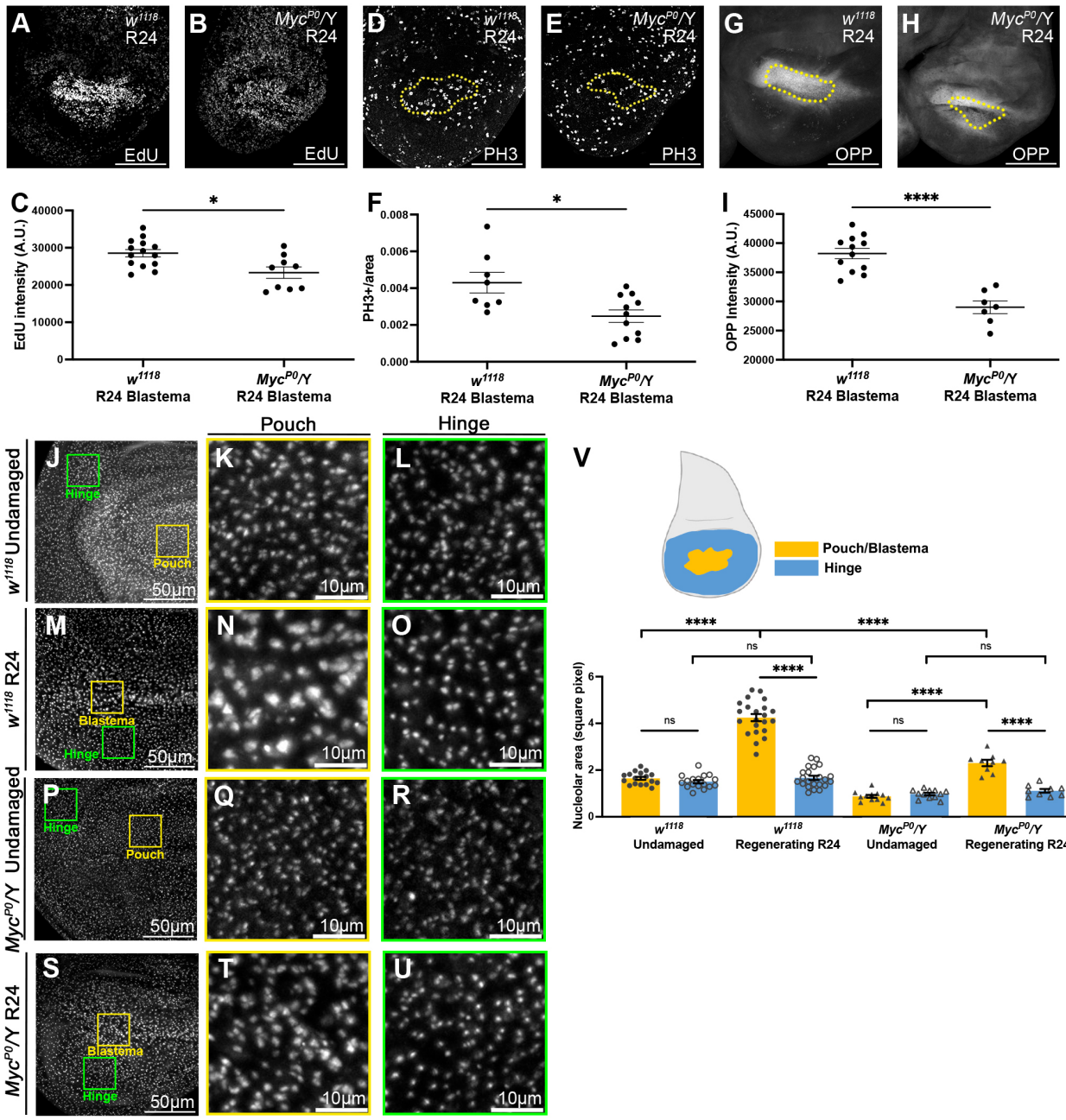
A
w1118
R24
EdU
B
MycP0/Y
R24
EdU
D
w1118
R24
PH3
E
MycP0/Y
R24
PH3
G
w1118
R24
OPP
H
MycP0/Y
R24
OPP
C
EdU intensity (A.U.)
40000
30000
20000
10000
0
*
w1118
R24 Blastema
MycP0/Y
R24 Blastema
F
PH3+/area
0.008
0.006
0.004
0.002
0.000
*
w1118
R24 Blastema
MycP0/Y
R24 Blastema
I
OPP Intensity (A.U.)
45000
40000
35000
30000
25000
20000
****
w1118
R24 Blastema
MycP0/Y
R24 Blastema
Pouch
Hinge
w1118 Undamaged
J
Hinge
Pouch
50µm
K
10µm
L
10µm
w1118 R24
M
Blastema
Hinge
50µm
N
10µm
O
10µm
MycP0/Y Undamaged
P
Hinge
Pouch
50µm
Q
10µm
R
10µm
MycP0/Y R24
S
Blastema
Hinge
50µm
T
10µm
U
10µm
V
Pouch/Blastema
Hinge
Nucleolar area (square pixel)
6
4
2
0
****
****
ns
ns
****
ns
****
ns
****
w1118
Undamaged
w1118
Regenerating R24
MycP0/Y
Undamaged
MycP0/Y
Regenerating R24

Figure 2. Myc promotes growth in the regeneration blastema

(A-B) EdU incorporation in a w^{1118} R24 disc (A) and a Myc^{P0}/Y R24 disc (B). (C) Quantification of average EdU intensity in the wing pouch identified by morphological features. w^{1118}n=14, Myc^{P0}/Y n=9. *P<0.05. (D-E) PH3 staining in a w^{1118} R24 disc (D) and a Myc^{P0}/Y R24 disc (E). (F) Quantification of mitotic cells per area in the blastema (Wg, yellow dotted lines in D-E). w^{1118} n=8, Myc^{P0}/Y n=11. *P<0.05. (G-H) OPP assay in a w^{1118} R24 disc (G) and a Myc^{P0}/Y R24 disc (H). (I) Quantification of average OPP signal in the Wg+ blastema. w^{1118} n=12, Myc^{P0}/Y n=7. ****P<0.0001. (J-U) Fibrillarin staining marking nucleoli in a w^{1118} undamaged disc (J-L), a w^{1118} R24 disc (M-O), a Myc^{P0}/Y undamaged disc (P-R), and a Myc^{P0}/Y R24 disc (S-U). (K,N,Q,T) 200-pixel square from pouch or Wg+ blastema (yellow boxes). (L,O,R,U) 200-pixel square from hinge (green boxes). (V) Quantification of nucleolus size. w^{1118} undamaged n=17, w^{1118} R24 n=22, Myc^{P0}/Y undamaged n=12, Myc^{P0}/Y R24 n=9. n.s. P>0.05, ****P<0.0001. Statistical test used was Welch's t-test. Scale bars are 100μm. Error bars are SEM.

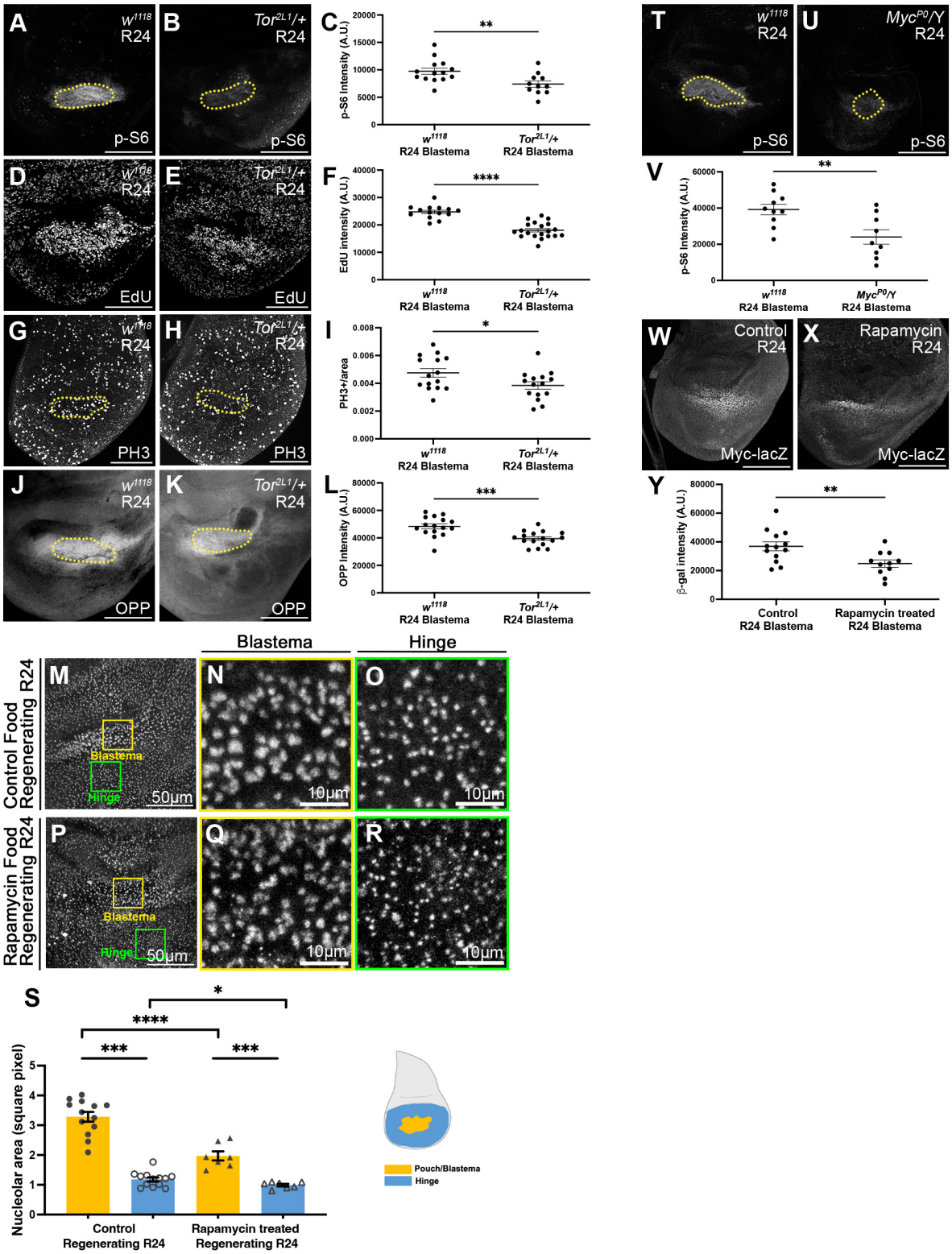
A
w1118
R24
p-S6
B
Tor2L1/+
R24
p-S6
C
p-S6 Intensity (A.U.)
**
w1118
R24 Blastema
Tor2L1/+
R24 Blastema
D
w1118
R24
EdU
E
Tor2L1/+
R24
EdU
F
EdU intensity (A.U.)
****
G
w1118
R24
PH3
H
Tor2L1/+
R24
PH3
I
PH3+/area
*
J
w1118
R24
OPP
K
Tor2L1/+
R24
OPP
L
OPP Intensity (A.U.)
***
T
w1118
R24
p-S6
U
MycP0/Y
R24
p-S6
V
p-S6 Intensity (A.U.)
**
MycP0/Y
R24 Blastema
W
Control
R24
Myc-lacZ
X
Rapamycin
R24
Myc-lacZ
Y
β-gal intensity (A.U.)
**
Control
R24 Blastema
Rapamycin treated
R24 Blastema
Blastema
Hinge
Control Food
Regenerating R24
M
Blastema
Hinge
50µm
N
10µm
O
10µm
Rapamycin Food
Regenerating R24
P
Blastema
Hinge
50µm
Q
10µm
R
10µm
S
Nucleolar area (square pixel)
*
****
***
***
Control
Regenerating R24
Rapamycin treated
Regenerating R24
Pouch/Blastema
Hinge

Figure 3. Tor promotes growth in the regeneration blastema

(A-B) p-S6 immunostaining in a w^{1118} R24 disc (A) and a Tor^{2L1}/+ R24 disc (B). (C) Quantification of average p-S6 staining intensity in the Wg+ blastema (yellow dotted lines). w^{1118} n=14, Tor^{2L1}/+ n=11. **P<0.01, Welch's t-test. (D-E) EdU incorporation in a w^{1118} R24 disc (D) and a Tor^{2L1}/+ R24 disc (E). (F) Quantification of average EdU staining intensity in the blastema identified by morphological features. w^{1118} n=14, Tor^{2L1}/+ n=20. ****P<0.0001. (G-H) PH3 staining in a w^{1118} R24 disc (G) and a Tor^{2L1}/+ R24 disc (H). (I) Quantification of mitotic cells per area in the Wg+ blastema (yellow dotted lines). w^{1118} n=15, Tor^{2L1}/+ n=15. *P<0.05. (J-K) OPP assay in a w^{1118} R24 disc (J) and a Tor^{2L1}/+ R24 disc (K). (L) Quantification of average OPP staining in the Wg+ blastema (yellow dotted lines). w^{1118} n=16, Tor^{2L1}/+ n=16. ***P<0.001. (M-S) Fibrillarin staining in an R24 disc after feeding with control food (M-O) or food containing rapamycin (P-R). (N,Q) 200-pixel squares from the Wg+ blastema (yellow boxes). (O,R) 200-pixel square from the hinge (green boxes). (S) Quantification of nucleolus size in hinge and blastema. control n=13, rapamycin n=7. *P<0.05, ***P<0.001, ****P<0.0001. (T-U) p-S6 staining in a w^{1118} (T) and a Myc^{P0}/Y (U) disc. (V) Quantification of average p-S6 staining intensity in Zone A identified by Wg staining (yellow dotted lines). w^{1118} n=10 , Myc^{P0}/Y n=9. **P<0.01. (W-Y) *Myc-lacZ* expression marked by β-gal staining in a control R24 disc (W) and a rapamycin-treated R24 disc (X). (Y) Quantification of average β-gal staining intensity in the blastema. control n=13, rapamycin n=11. **P<0.01. Statistical test used was Welch's t-test. Scale bars are 100μm unless otherwise marked. Error bars are SEM.

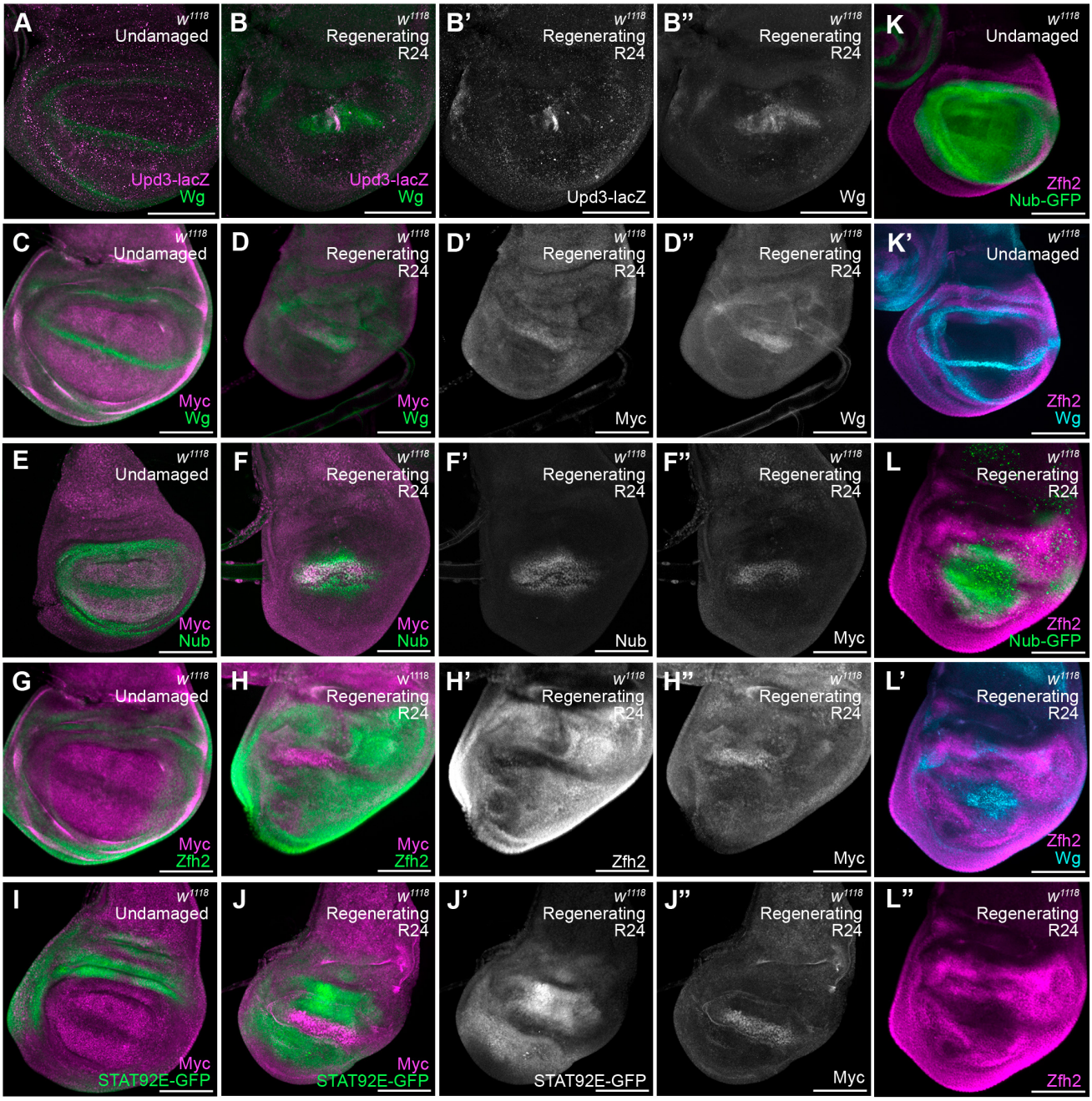
A
w1118
Undamaged
Upd3-lacZ
Wg
B
w1118
Regenerating
R24
Upd3-lacZ
Wg
B'
w1118
Regenerating
R24
Upd3-lacZ
B''
w1118
Regenerating
R24
Wg
K
w1118
Undamaged
Zfh2
Nub-GFP
C
w1118
Undamaged
Myc
Wg
D
w1118
Regenerating
R24
Myc
Wg
D'
w1118
Regenerating
R24
Myc
D''
w1118
Regenerating
R24
Wg
K'
w1118
Undamaged
Zfh2
Wg
E
w1118
Undamaged
Myc
Nub
F
w1118
Regenerating
R24
Myc
Nub
F'
w1118
Regenerating
R24
Nub
F''
w1118
Regenerating
R24
Myc
L
w1118
Regenerating
R24
Zfh2
Nub-GFP
G
w1118
Undamaged
Myc
Zfh2
H
w1118
Regenerating
R24
Myc
Zfh2
H'
w1118
Regenerating
R24
Zfh2
H''
w1118
Regenerating
R24
Myc
L'
w1118
Regenerating
R24
Zfh2
Wg
I
w1118
Undamaged
Myc
STAT92E-GFP
J
w1118
Regenerating
R24
Myc
STAT92E-GFP
J'
w1118
Regenerating
R24
STAT92E-GFP
J''
w1118
Regenerating
R24
Myc
L''
w1118
Regenerating
R24
Zfh2

822 **Figure 4. Mapping the domain of Myc expression in the regeneration blastema**
823 (A-B”) Wg immunostaining and *upd-lacZ* expression detected by β-Gal immunostaining
824 in an undamaged disc (A) and an R24 disc (B-B”). (C-D”) Myc and Wg immunostaining
825 in an undamaged disc (C) and an R24 disc (D-D”). (E-F”) Nub and Wg immunostaining
826 in an undamaged disc (E) and an R24 disc (F-F”). (G-H’) Zfh2 and Wg immunostaining
827 in an undamaged disc (G) and an R24 disc (H-H”). (I-J”) *STAT92E-GFP* expression and
828 Wg staining in an undamaged disc (I) and an R24 disc (J-J”). (K-L”) Zfh2 and Wg
829 staining as well as *nub-GFP* expression in an undamaged disc (K-K’) and an R24 disc
830 (L-L”). Scale bars are 100μm.
831
832

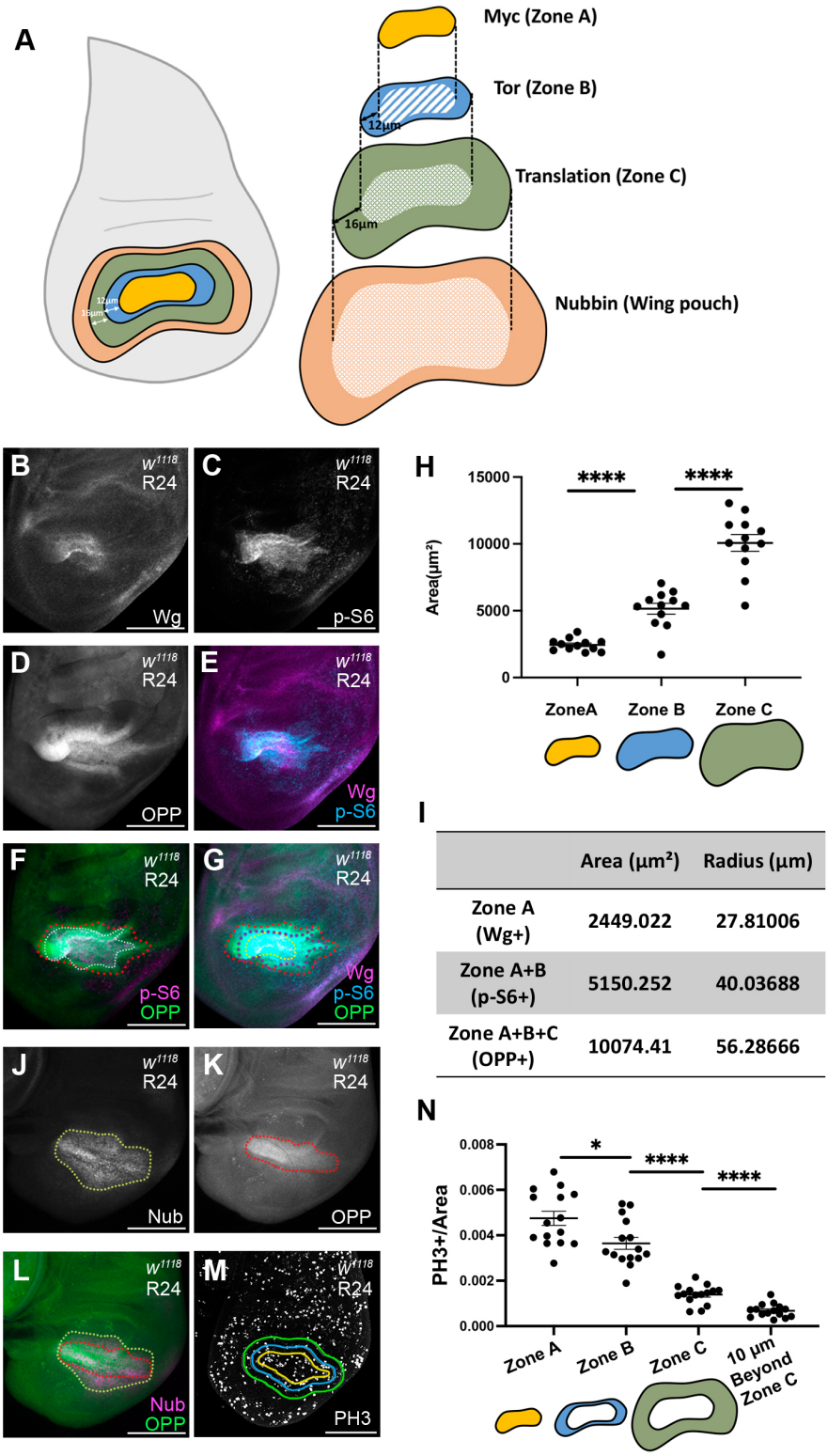

I

	Area (µm²)	Radius (µm)
Zone A (Wg+)	2449.022	27.81006
Zone A+B (p-S6+)	5150.252	40.03688
Zone A+B+C (OPP+)	10074.41	56.28666

833 **Figure 5. Zones of growth in the regeneration blastema**

834 (A) Schematic of concentric growth zones in a regenerating wing disc. (B-G) Wg
835 staining (yellow dashed line), p-S6 staining (white dashed line) and OPP assay (red
836 dashed line) in the same R24 disc. (B) Wg. (C) p-S6. (D) OPP assay. (E) Wg and p-S6.
837 (F) Wg and OPP assay. (G) Wg, p-S6, and OPP assay. (H) Quantification of area in
838 zones identified by Wg, p-S6, and the OPP assay. n=12. ****P<0.0001, Welch's t-test.
839 (I) Average area and radius of each zone. (J-L) R24 disc with Nub staining (J), OPP
840 assay (K), and merged image (L). (M) PH3 staining in an R24 disc. Yellow line outlines
841 Growth Zone A. Blue line outlines Growth Zone B, 13 microns beyond Growth Zone A.
842 Green line outlines Growth Zone C, 16 microns beyond Growth Zone B. (N)
843 Quantification of mitotic cells per area in each growth zone identified as in (M). n=15.
844 *P<0.05, ****P<0.0001, Welch's t-test. Scale bars are 100μm. Error bars are SEM.
845
846

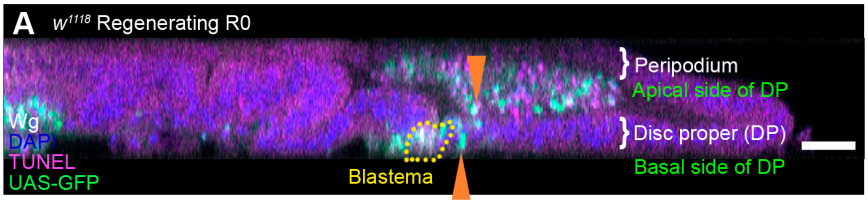
A
w1118 Regenerating R0
Peripodium
Apical side of DP
Disc proper (DP)
Basal side of DP
Wg
DAPI
TUNEL
UAS-GFP
Blastema

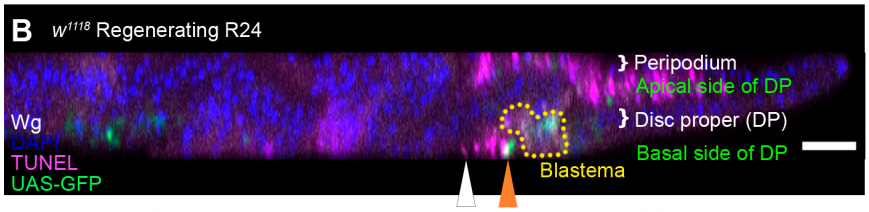
B
w1118 Regenerating R24
Peripodium
Apical side of DP
Disc proper (DP)
Basal side of DP
Wg
DAPI
TUNEL
UAS-GFP
Blastema

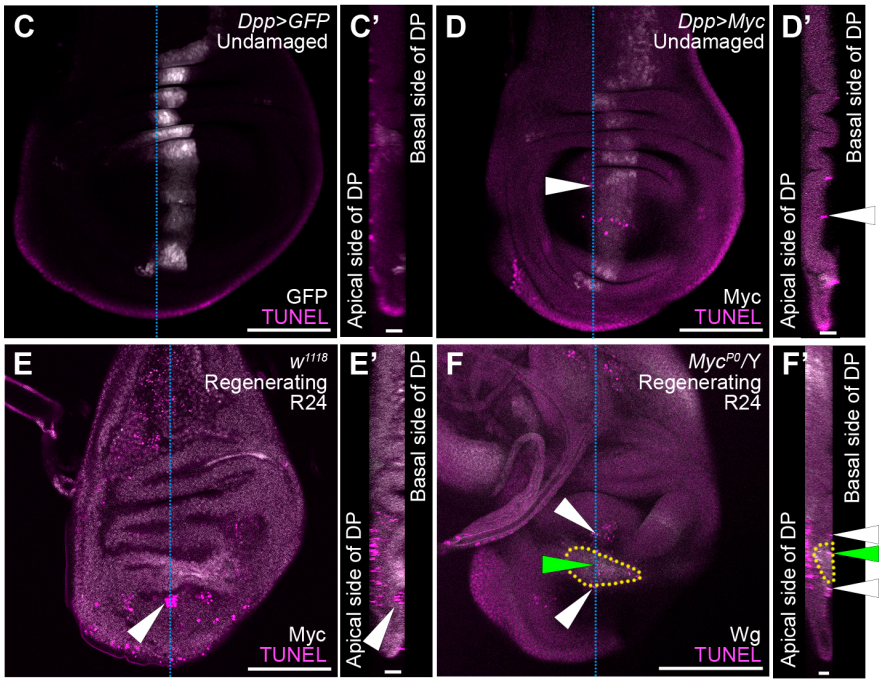
C
Dpp>GFP
Undamaged
GFP
TUNEL
C'
Apical side of DP
Basal side of DP
D
Dpp>Myc
Undamaged
Myc
TUNEL
D'
Apical side of DP
Basal side of DP
E
w1118
Regenerating
R24
Myc
TUNEL
E'
Apical side of DP
Basal side of DP
F
MycP0/Y
Regenerating
R24
Wg
TUNEL
F'
Apical side of DP
Basal side of DP

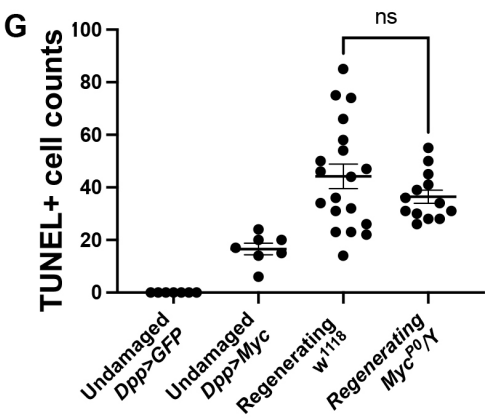
G
TUNEL+ cell counts
100
80
60
40
20
0
ns
Undamaged Dpp>GFP
Undamaged Dpp>Myc
Regenerating w1118
Regenerating MycP0/Y

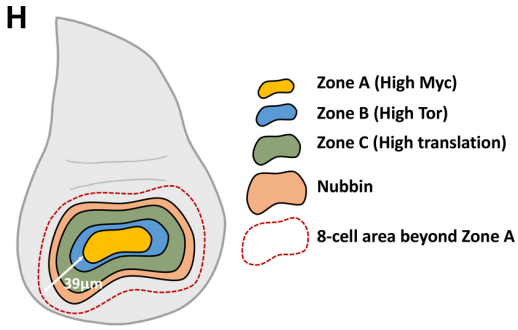
H
Zone A (High Myc)
Zone B (High Tor)
Zone C (High translation)
Nubbin
8-cell area beyond Zone A
39µm

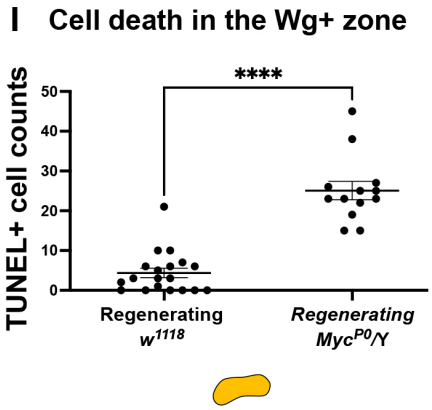
I
Cell death in the Wg+ zone
TUNEL+ cell counts
50
40
30
20
10
0
****
Regenerating w1118
Regenerating MycP0/Y

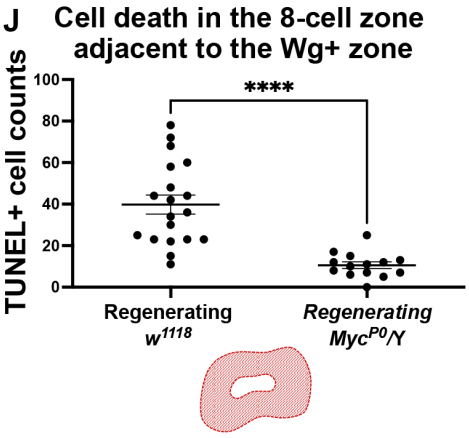
J
Cell death in the 8-cell zone adjacent to the Wg+ zone
TUNEL+ cell counts
100
80
60
40
20
0
****
Regenerating w1118
Regenerating MycP0/Y

847 **Figure 6. Myc expression induces cell death at the periphery of Growth Zone A**
848 (A-B) Orthogonal views of an R0 disc (A) and an R24 disc (B). Wg staining (white)
849 marks the regeneration blastema (yellow dotted lines). UAS-GFP (green) marks cell
850 debris from tissue ablation. TUNEL assay (magenta) marks debris and apoptotic cells.
851 DAPI (blue) marks nuclei. White arrowhead marks TUNEL+ GFP- apoptotic cell, orange
852 arrowhead marks TUNEL+ GFP+ cell debris. (C-F) TUNEL assay marking apoptotic
853 cells in a negative control (*dpp-Gal4>UASGFP*) (C), positive control
854 (*dppGal4>UASMyc*) (D), w^{1118} R24 disc (E), and Myc^{P0}/Y R24 disc (F). (E) w^{1118} R24
855 disc with Myc staining marking Growth Zone A. (F) Myc^{P0}/Y R24 disc with Wg staining
856 (yellow line) marking Growth Zone A. (C',D',E',F') Orthogonal views of (C,D,E,F). White
857 arrowheads mark apoptosis adjacent to high Myc expression. Green arrowhead marks
858 apoptosis in the blastema. (G) Quantification of cell death labeled by TUNEL at the
859 basal side of the epithelium in the areas that were GFP+ (C) or Myc+ (D) in the wing
860 pouch and an eight-cell band extending anteriorly, or the Wg+ Myc+ blastema and an
861 eight-cell band outside of the blastema. *dpp>GFP* n=7*, dpp>Myc* n=7*,* w^{1118} R24 n=19,
862 Myc^{P0}/Y R24 n=14. n.s. P>0.05. (H) Schematic of a regenerating wing disc, yellow
863 indicates the Wg+Myc+ zone (Growth Zone A), blue indicates Growth Zone B, green
864 indicates Growth Zone C, red dashed line indicates the eight-cell diameter region
865 beyond Zone A. (I) Quantification of cell death in the Wg+ zone in R24 discs. w^{1118}
866 n=19, Myc^{P0}/Y n=14. ****P<0.0001, Welch's t-test. (J) Quantification of cell death in the
867 eight-cell band outside the Wg+ zone. w^{1118} n=19, Myc^{P0}/Y n=14. ****P<0.0001. Scale
868 bars are 100μm. Error bars are SEM. Statistical test used was Welch's t-test.
869
870
871

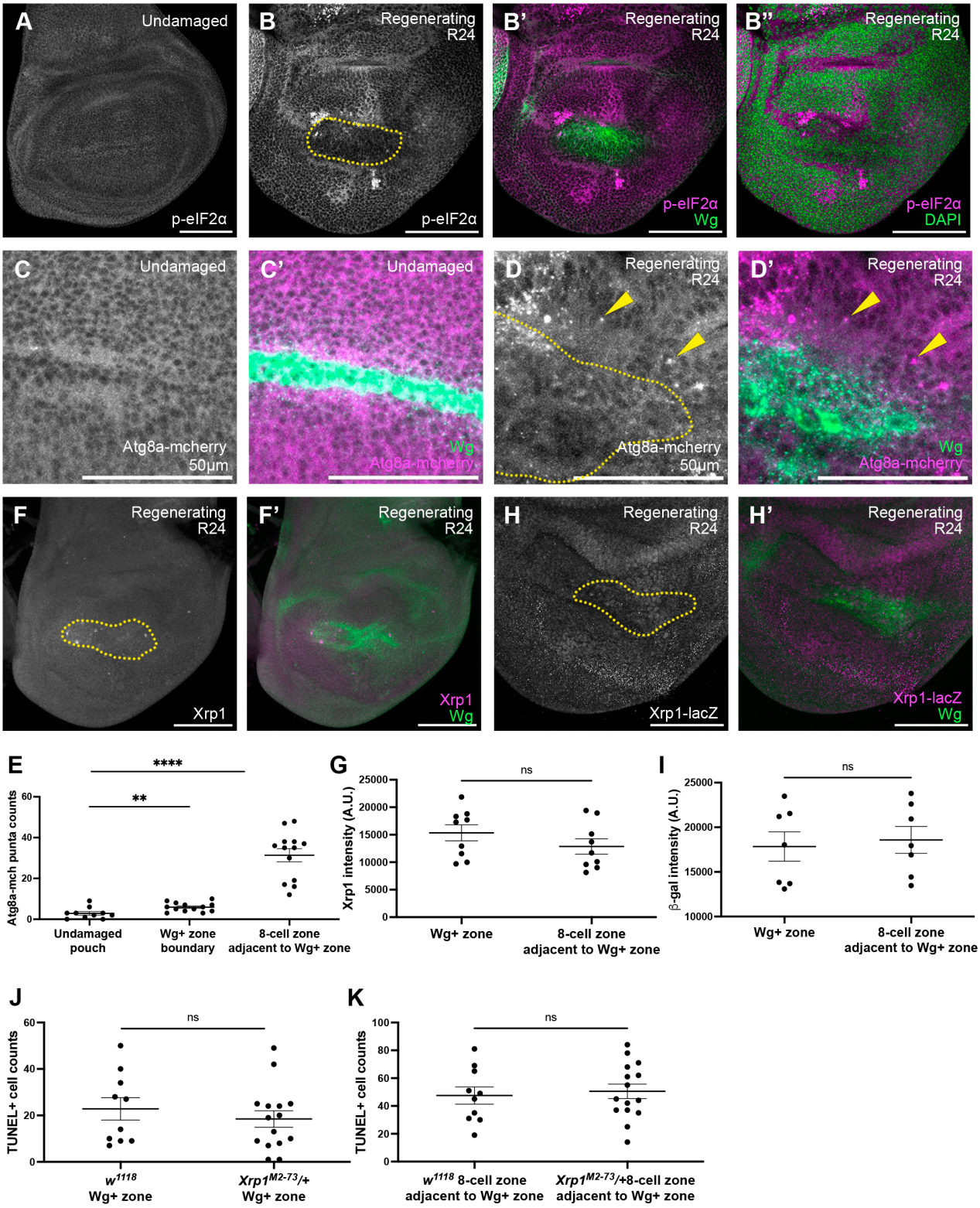
A
Undamaged
p-eIF2α
B
Regenerating R24
p-eIF2α
B'
Regenerating R24
p-eIF2α
Wg
B''
Regenerating R24
p-eIF2α
DAPI
C
Undamaged
Atg8a-mcherry
50μm
C'
Undamaged
Wg
Atg8a-mcherry
D
Regenerating R24
Atg8a-mcherry
50μm
D'
Regenerating R24
Wg
Atg8a-mcherry
F
Regenerating R24
Xrp1
F'
Regenerating R24
Xrp1
Wg
H
Regenerating R24
Xrp1-lacZ
H'
Regenerating R24
Xrp1-lacZ
Wg
E
Atg8a-mch punta counts
****
**
Undamaged pouch
Wg+ zone boundary
8-cell zone adjacent to Wg+ zone
G
Xrp1 intensity (A.U.)
ns
Wg+ zone
8-cell zone adjacent to Wg+ zone
I
β-gal intensity (A.U.)
ns
Wg+ zone
8-cell zone adjacent to Wg+ zone
J
TUNEL+ cell counts
ns
w1118 Wg+ zone
Xrp1M2-73/+ Wg+ zone
K
TUNEL+ cell counts
ns
w1118 8-cell zone adjacent to Wg+ zone
Xrp1M2-73/+8-cell zone adjacent to Wg+ zone

872 **Figure 7. Cell competition induced in regenerating wing discs is distinct from**
873 **experimentally induced cell competition**
874 (A-B) p-eIF2α staining in an undamaged disc (A) and an R24 disc (B). (B') p-eIF2α and
875 Wg. (B") p-eIF2α and DAPI. (C-D) Atg8a-mcherry expression in an undamaged disc (C)
876 and an R24 disc (D). (C'-D') Atg8a-mcherry expression and Wg staining (yellow circle in
877 C, D). Arrowheads indicate Atg8a puncta. Note that (C-D') are 250-pixel^2 area cropped
878 from FigS6 (A-B) to better show the puncta. (E) Quantification of Atg8a puncta. n=13.
879 **P<0.01, ****P<0.0001. (F-F') Xrp1 staining in an R24 disc. Yellow dotted circle
880 indicates blastema marked by Wg. (G) Quantification of Xrp1 intensity. n=9, n.s.
881 P>0.05. (H-H') *Xrp1-lacZ* expression in an R24 disc. Yellow dotted circle indicates
882 blastema marked by Wg. (I) Quantification of average β-gal staining intensity. n=7, n.s.
883 P>0.05. (J-K) Quantification of cell death (TUNEL) in the Wg+ area (J) and in the 8-cell
884 zone adjacent to the Wg+ area (K) in w^{1118} R24 discs and $Xrp1^{M2-73}$/+ R24 discs. w^{1118}
885 n=10, $Xrp1^{M2-73}$/+ n=15. n.s. P>0.05. Scale bars are 100μm. Error bars are SEM.
886 Statistical test used was Welch's t-test.
887
888

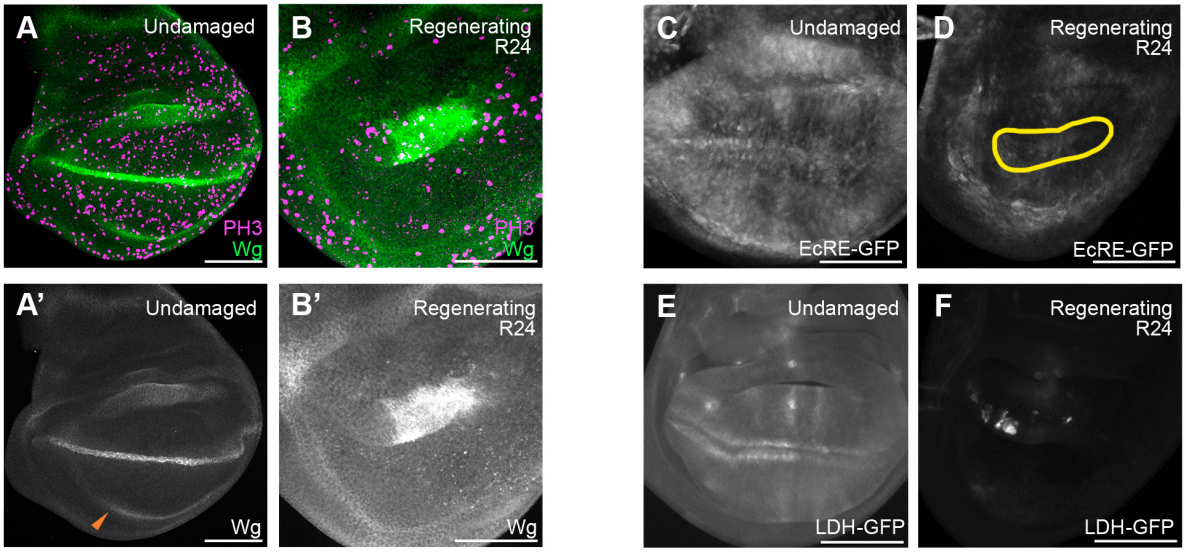
A
Undamaged
PH3
Wg
B
Regenerating
R24
PH3
Wg
C
Undamaged
EcRE-GFP
D
Regenerating
R24
EcRE-GFP
A'
Undamaged
Wg
B'
Regenerating
R24
Wg
E
Undamaged
LDH-GFP
F
Regenerating
R24
LDH-GFP

889 **Figure S1. Ecdysone receptor and Lactate dehydrogenase do not drive**
890 **regenerative growth**
891 (A-B') PH3 staining in an undamaged disc (A-A') and an R24 disc (B-B'). Orange
892 arrowhead in (A') indicates inner ring of Wg. (C-D) EcRE-GFP expression in an
893 undamaged disc (C) and an R24 disc (D). (E-F) LDH-GFP expression in an undamaged
894 disc (E) and an R24 disc (F).
895

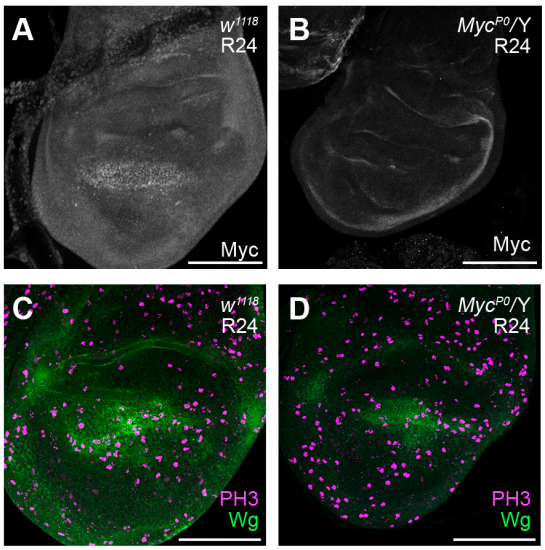
A
w1118
R24
Myc
B
MycP0/Y
R24
Myc
C
w1118
R24
PH3
Wg
D
MycP0/Y
R24
PH3
Wg

896 **Figure S2. The *Myc^{P0}* mutation reduces Myc and proliferation during regeneration**

897 (A-B) Myc immunostaining in a *w^{1118}* R24 disc (A) and a *Myc^{P0}/Y* R24 disc (B). (C-D)

898 PH3 staining in a *w^{1118}* R24 disc (C) and a *Myc^{P0}/Y* R24 disc (D).

899

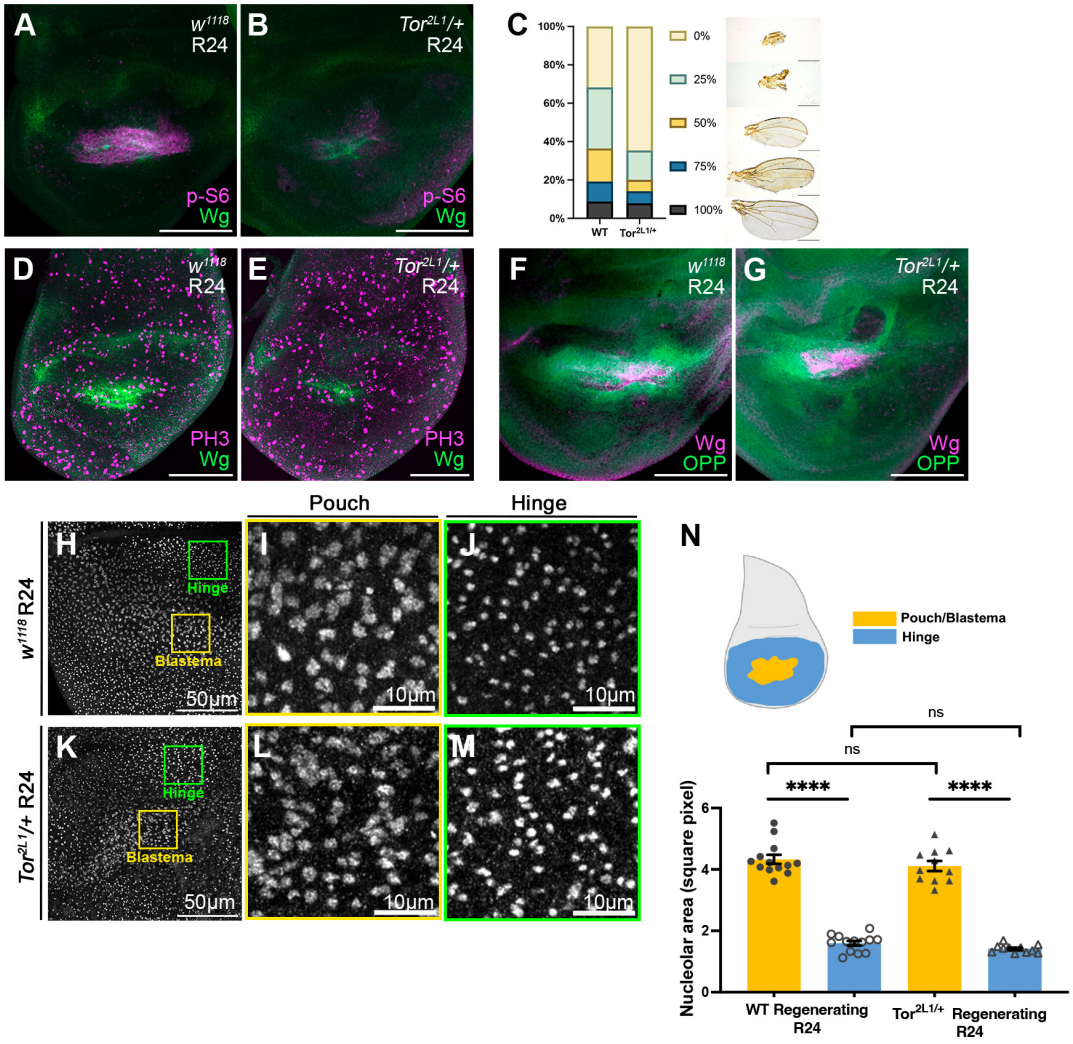
A
w1118
R24
p-S6
Wg
B
Tor2L1/+
R24
p-S6
Wg
C
100%
80%
60%
40%
20%
0%
WT
Tor2L1/+
0%
25%
50%
75%
100%
D
w1118
R24
PH3
Wg
E
Tor2L1/+
R24
PH3
Wg
F
w1118
R24
Wg
OPP
G
Tor2L1/+
R24
Wg
OPP
Pouch
Hinge
w1118 R24
H
Hinge
Blastema
50µm
I
10µm
J
10µm
Tor2L1/+ R24
K
Hinge
Blastema
50µm
L
10µm
M
10µm
N
Pouch/Blastema
Hinge
ns
ns
****
****
Nucleolar area (square pixel)
6
4
2
0
WT Regenerating R24
Tor2L1/+ Regenerating R24

900 **Figure S3. Effects of the *Tor^{2L1}* mutation on regeneration.**

901 (A-B) p-S6 and Wg staining in a *w^{1118}* R24 disc (A) and a *Tor^{2L1}*/+ R24 disc (B). (C) Size
902 of adult wings after disc regeneration in *w^{1118}* and *Tor^{2L1}*/+ animals. Scale bars are
903 500µm. (D-E) PH3 staining in a *w^{1118}* R24 disc (D) and a *Tor^{2L1}*/+ R24 disc (E). (F-G)
904 OPP assay with Wg staining in a *w^{1118}* R24 disc (F) and a *Tor^{2L1}*/+ R24 disc (G). (H-M)
905 Fibrillarin staining marking nucleoli in a *w^{1118}* R24 disc (H-J) and a *Tor^{2L1}*/+ R24 disc (K-
906 M). (I, L) 200-pixel^2 area from blastema in H, K accordingly (yellow boxes), identified by
907 Wg staining. (J, M) 200-pixel^2 area from wing hinge in H, K (green boxes). (N)
908 Quantification of nucleolus size in hinge and blastema. *w^{1118}* n=13, *Tor^{2L1}*/+ n=11.
909 ****P<0.0001, n.s. P>0.05. Scale bars are 100µm unless otherwise marked. Error bars
910 are SEM. Statistical test used was Welch's t-test.

911

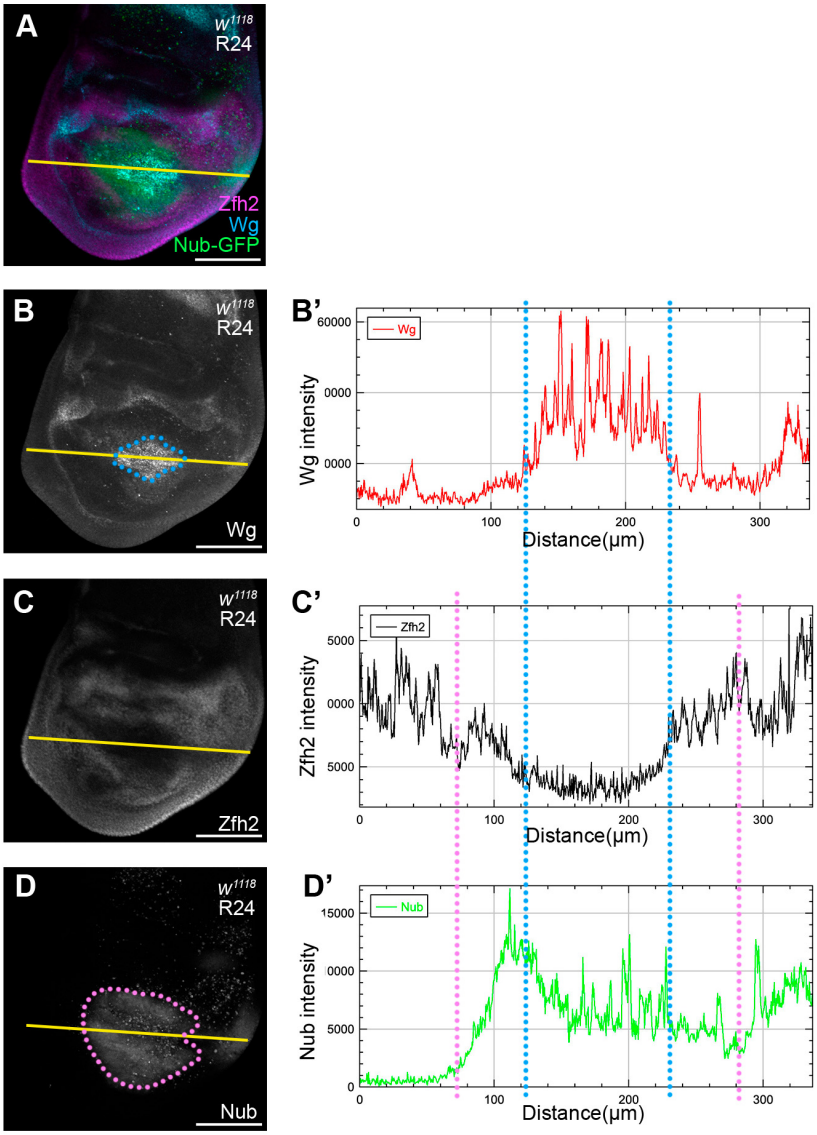
A
w1118
R24
Zfh2
Wg
Nub-GFP
B
w1118
R24
Wg
B'
Wg
Wg intensity
60000
0000
0000
0
100
200
300
Distance(μm)
C
w1118
R24
Zfh2
C'
Zfh2
Zfh2 intensity
5000
0000
5000
0
100
200
300
Distance(μm)
D
w1118
R24
Nub
D'
Nub
Nub intensity
15000
0000
5000
0
0
100
200
300
Distance(μm)

912 **Figure S4. Map of Zfh2, Wg, and Nub expression.**

913 (A) R24 disc expressing *nub-GFP* with Zfh2 and Wg immunostaining. (B) Wg staining.
914 (B') Intensity plot of Wg staining taken from the yellow cross-section line in (B). (C) Zfh2
915 staining. (C') Intensity plot of Zfh2 staining taken from the yellow cross-section line in
916 (C). (D) *nub-GFP* expression. (D') Intensity plot of GFP taken from the yellow cross-
917 section line in (D). Blue dotted circle in (B) and blue dotted lines in (B'-D') indicate the
918 edge of Wg-expressing area. Pink dotted circle in (D) and pink dotted lines in (C'-D')
919 indicate edge of *nub-GFP* expressing area. Scale bars are 100μm.

920

921

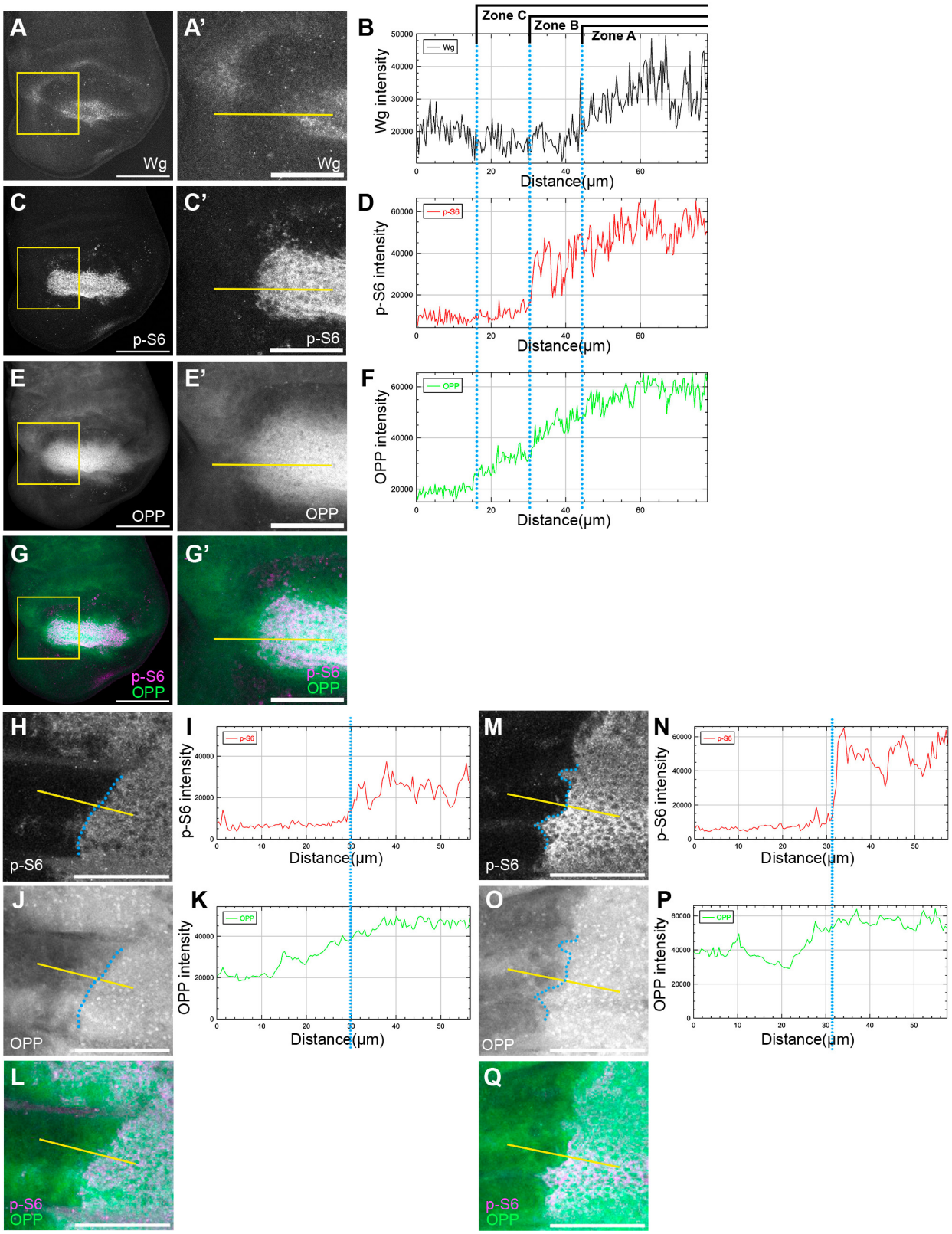
A
Wg
A'
Wg
B
Zone C
Zone B
Zone A
Wg
Wg intensity
Distance(μm)
C
p-S6
C'
p-S6
D
p-S6
p-S6 intensity
Distance(μm)
E
OPP
E'
OPP
F
OPP
OPP intensity
Distance(μm)
G
p-S6
OPP
G'
p-S6
OPP
H
p-S6
I
p-S6
p-S6 intensity
Distance(μm)
M
p-S6
N
p-S6
p-S6 intensity
Distance(μm)
J
OPP
K
OPP
OPP intensity
Distance(μm)
O
OPP
P
OPP
OPP intensity
Distance(μm)
L
p-S6
OPP
Q
p-S6
OPP

922 **Figure S5. Map of Wg, p-S6, and OPP in the blastema.**

923 (A,C,E,G) A *w*^{1118} R24 disc with Wg (A) and p-S6 (C) staining, OPP assay (E), and
924 merge of p-S6 and OPP (G). (A',C',E',G') A higher magnification image of the yellow
925 square in (A-G). (B,D,F) Fluorescence intensity plots taken from the yellow line in
926 (A',C',E'). (H-Q) *hhGal4, UAS-Tsc2RNAi* (*hh>Tsc2i*) undamaged discs with p-S6
927 immunostaining (H, M) and OPP assay (J, O). Note (H-K) are from one wing disc and
928 (M-Q) are from another wing disc. (I) Fluorescence intensity plot taken from the yellow
929 line in (H). (K) Fluorescence intensity plot taken from the yellow line in (J). (N)
930 Fluorescence intensity plot taken from the yellow line in (M). (O) Fluorescence intensity
931 plot taken from the yellow line in (P). Blue dotted lines in (H-K) and (M-P) indicate the
932 edge between high/low p-S6 staining. Scale bars are 100μm.

933

934

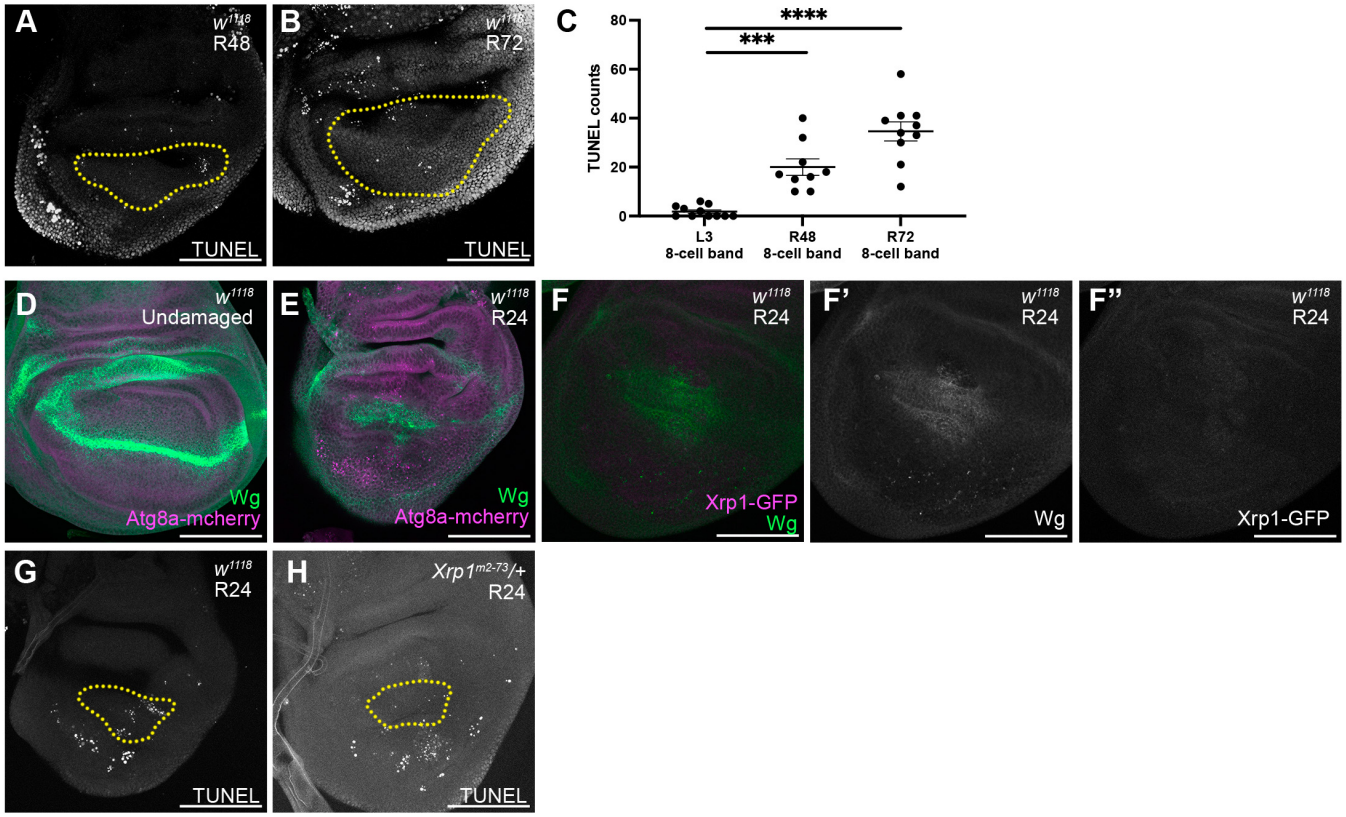
A
w1118
R48
TUNEL
B
w1118
R72
TUNEL
C
****
***
TUNEL counts
80
60
40
20
0
L3
8-cell band
R48
8-cell band
R72
8-cell band
D
w1118
Undamaged
Wg
Atg8a-mcherry
E
w1118
R24
Wg
Atg8a-mcherry
F
w1118
R24
Xrp1-GFP
Wg
F'
w1118
R24
Wg
F''
w1118
R24
Xrp1-GFP
G
w1118
R24
TUNEL
H
Xrp1m2-73/+
R24
TUNEL

935 **Figure S6. Cell death at later time points and expression of Atg8a and Xrp1-GFP.**
936 (A-B) TUNEL assay marking apoptotic cells in an R48 wing disc (A) and an R72 wing
937 disc (B). Yellow dotted circle indicates Zone A marked by Myc. (C) Quantification of cell
938 death (TUNEL) in the 8-cell zone adjacent to the Myc+ area. L3 n=11, R48 n=9, R72
939 n=10. ***P<0.001, ****P<0.0001. Error bars are SEM. Statistical test used was Welch's
940 t-test. (D-E) Atg8a-mcherry expression in an undamaged disc (D) and an R24 disc (E).
941 (F-F") Xrp1-GFP expression in wing disc with Wg staining. (F) merge, (F') Wg, (F'')
942 GFP. (G-H) TUNEL assay marking apoptotic cells in a w^{1118} R24 disc (G) and a $Xrp1^{M2-}$
943 ^{73}/+ disc (H). Yellow dotted circle indicates Growth Zone A marked by Wg. Scale bars
944 are 100μm.
945
946

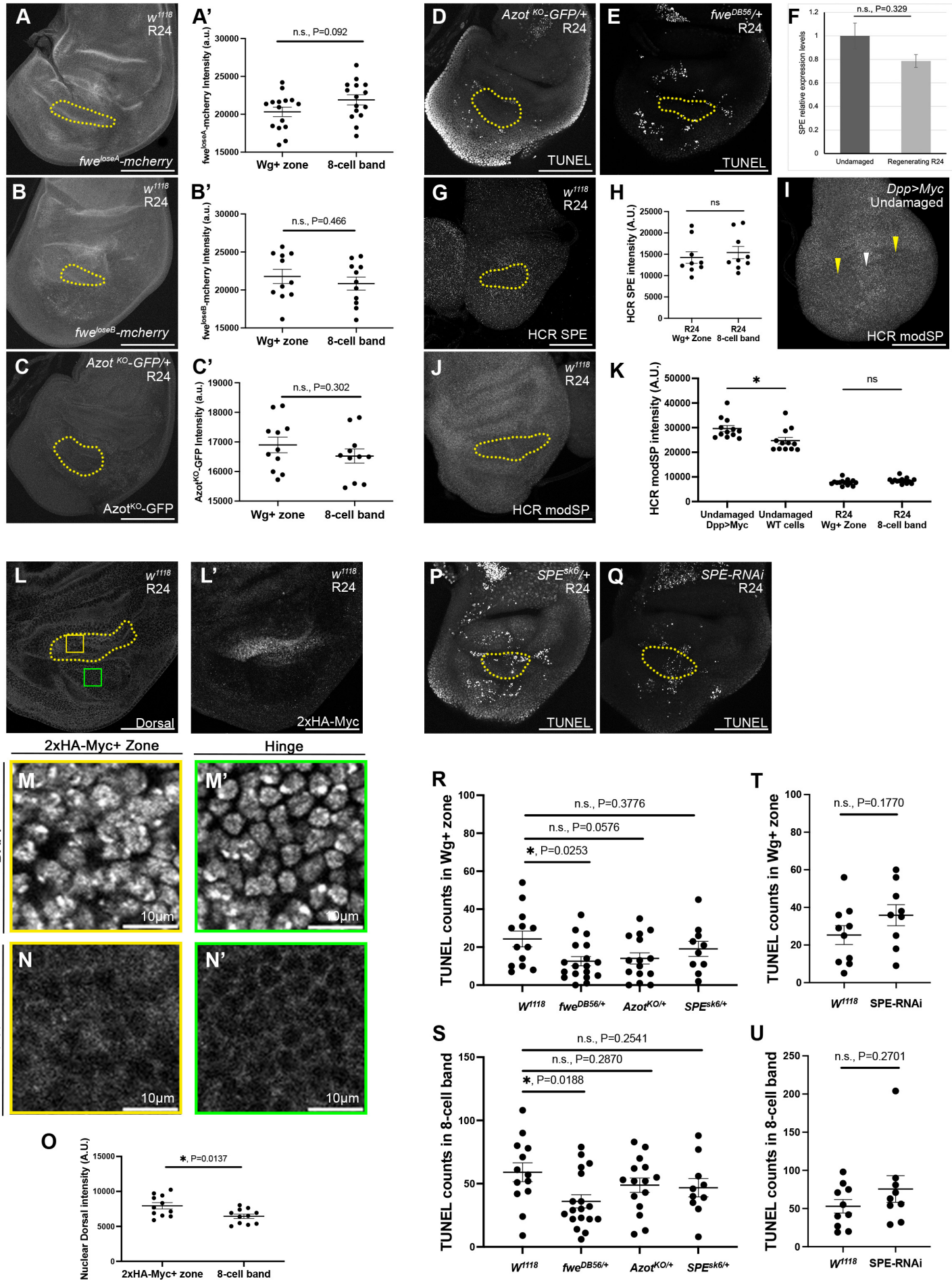
A
w1118
R24
fweloseA-mcherry
A'
n.s., P=0.092
fweloseA-mcherry Intensity (a.u.)
Wg+ zone
8-cell band
B
w1118
R24
fweloseB-mcherry
B'
n.s., P=0.466
fweloseB-mcherry Intensity (a.u.)
Wg+ zone
8-cell band
C
Azot KO-GFP/+
R24
AzotKO-GFP
C'
n.s., P=0.302
AzotKO-GFP Intensity (a.u.)
Wg+ zone
8-cell band
D
Azot KO-GFP/+
R24
TUNEL
E
fweDB56/+
R24
TUNEL
F
n.s., P=0.329
SPE relative expression levels
Undamaged
Regenerating R24
G
w1118
R24
HCR SPE
H
ns
HCR SPE intensity (A.U.)
R24 Wg+ Zone
R24 8-cell band
I
Dpp>Myc
Undamaged
HCR modSP
J
w1118
R24
HCR modSP
K
*
ns
HCR modSP intensity (A.U.)
Undamaged Dpp>Myc
Undamaged WT cells
R24 Wg+ Zone
R24 8-cell band
L
w1118
R24
Dorsal
L'
w1118
R24
2xHA-Myc
2xHA-Myc+ Zone
Hinge
DAPI
Dorsal
M
M'
N
N'
10µm
O
*, P=0.0137
Nuclear Dorsal intensity (A.U.)
2xHA-Myc+ zone
8-cell band
P
SPEsk6/+
R24
TUNEL
Q
SPE-RNAi
R24
TUNEL
R
n.s., P=0.3776
n.s., P=0.0576
*, P=0.0253
TUNEL counts in Wg+ zone
W1118
fweDB56/+
AzotKO/+
SPEsk6/+
T
n.s., P=0.1770
TUNEL counts in Wg+ zone
W1118
SPE-RNAi
S
n.s., P=0.2541
n.s., P=0.2870
*, P=0.0188
TUNEL counts in 8-cell band
W1118
fweDB56/+
AzotKO/+
SPEsk6/+
U
n.s., P=0.2701
TUNEL counts in 8-cell band
W1118
SPE-RNAi

947 **Figure S7. Azot expression and Toll signaling do not regulate cell competition**
948 **during regeneration.**
949 (A) *fwe*^{loseA}-mcherry expression in an R24 disc. (A') Quantification of average mCherry
950 intensity. n=15. (B) *fwe*^{loseB}-mcherry expression in an R24 disc. (B') Quantification of
951 average mCherry intensity. n=11. (C) *azot*^{KO}*-GFP* expression in an R24 disc. (C')
952 Quantification of average GFP intensity. n=11. (D-E) TUNEL assay marking apoptotic
953 cells in an *azot*$^{KO-GFP}$/+ disc (D) and an *fwe*^{DB56}/+ disc (E). (F) RT-qPCR of SPE in
954 undamaged and R24 wing discs. (G) HCR of *SPE* in an R24 disc. (H) Quantification of
955 *SPE* intensity n=9. n.s. p>0.05. (I-J) HCR of *modSP* in an undamaged Dpp>Myc wing
956 disc (I) and an R24 wing disc (J). (I) White arrowhead marks the high-Myc cells and
957 yellow arrowheads mark the wildtype cells. (K) Quantification of *modSP* intensity.
958 Dpp>Myc n=12. R24 *w*^{1118} n=14. n.s. p>0.05, *p<0.05. (L-N') A R24 wing disc with
959 Dorsal staining (L) and with 2xHA-Myc (L'). Yellow dotted circle indicates Growth Zone
960 A marked by 2xHA-Myc+ cells. (M, N) 100-pixel^2 area from Zone A in (L) (yellow box)
961 with DAPI staining (M) and Dorsal staining (N). (M', N') 100-pixel^2 area from the 8-cell
962 zone in (L) (green box) with DAPI staining (M') and Dorsal staining (N'). (O)
963 Quantification of Dorsal intensity in Growth Zone A and in the 8-cell zone adjacent to
964 Growth Zone A. n=11. *p<0.05. (P-Q) TUNEL assay marking apoptotic cells in an
965 *SPE*^{sk6}/+ disc (P) and an *SPE-RNAi* disc (Q). (R) Quantification of cell death in the Wg+
966 Zone A. (S) Quantification of cell death in the eight-cell band outside Zone A in R24
967 discs. *w*^{1118} n=13, *fwe*^{DB56}/+ n=18, *azot* ^{KO}/+ n=15, *SPE*^{sk6}/+ n=10. (T) Quantification of
968 cell death in the Wg+ Zone A. *w*^{1118} n=10, *SPE-RNAi* n=9. (U) Quantification of cell
969 death in the eight-cell band outside Zone A in R24 discs. *w*^{1118} n=10, *SPE-RNAi* n=9.
970 Yellow dotted circle in A-E, G, J, P-Q indicates growth zone A marked by Wg. Scale
971 bars are 100μm unless otherwise marked. Error bars are SEM. Statistical tests were
972 Welch's t-test.
973
974

975 **Abbott, L. C., Karpen, G. H. and Schubiger, G.** (1981). Compartmental restrictions and blastema formation during
976 pattern regulation in Drosophila imaginal leg discs. *Dev Biol* **87**, 64–75.

977 **Abidi, S. N. F., Hsu, F. T.-Y. and Smith-Bolton, R. K.** (2023). Regenerative growth is constrained by brain tumor to
978 ensure proper patterning in Drosophila. *PLoS Genet* **19**, e1011103.

979 **Alpar, L., Bergantiños, C. and Johnston, L. A.** (2018). Spatially Restricted Regulation of Spätzle/Toll Signaling during
980 Cell Competition. *Dev Cell* **46**, 706-719.e5.

981 **Amoyel, M. and Bach, E. A.** (2014). Cell competition: How to eliminate your neighbours. *Development (Cambridge)*
982 **141**, 988–1000.

983 **Ascanelli, C., Dahir, R. and Wilson, C. H.** (2024). Manipulating Myc for reparative regeneration. *Front Cell Dev Biol*
984 **12**,.

985 **Baillon, L., Germani, F., Rockel, C., Hilchenbach, J. and Basler, K.** (2018). Xrp1 is a transcription factor required for
986 cell competition-driven elimination of loser cells. *Sci Rep* **8**, 17712.

987 **Baker, N. E.** (2020). Emerging mechanisms of cell competition. *Nat Rev Genet* **21**, 683–697.

988 **Baumgartner, M. E., Dinan, M. P., Langton, P. F., Kucinski, I. and Piddini, E.** (2021). Proteotoxic stress is a driver of
989 the loser status and cell competition. *Nat Cell Biol* **23**, 136–146.

990 **Bawa, S., Brooks, D. S., Neville, K. E., Tipping, M., Sagar, M. A., Kollhoff, J. A., Chawla, G., Geisbrecht, B. V,**
991 **Tennessen, J. M., Eliceiri, K. W., et al.** (2020). Drosophila TRIM32 cooperates with glycolytic enzymes to
992 promote cell growth. *Elife* **9**,.

993 **Bellen, H. J., Levis, R. W., Liao, G., He, Y., Carlson, J. W., Tsang, G., Evans-Holm, M., Hiesinger, P. R., Schulze, K. L.,**
994 **Rubin, G. M., et al.** (2004). The BDGP Gene Disruption Project. *Genetics* **167**, 761–781.

995 **Bellosta, P. and Gallant, P.** (2010). Myc Function in Drosophila. *Genes Cancer* **1**, 542–546.

996 **Bergantiños, C., Corominas, M. and Serras, F.** (2010). Cell death-induced regeneration in wing imaginal discs
997 requires JNK signalling. *Development* **137**, 1169–1179.

998 **Blanco, J., Cooper, J. C. and Baker, N. E.** (2020). Roles of C/EBP class bZip proteins in the growth and cell competition
999 of Rp ('Minute') mutants in Drosophila. *Elife* **9**,.

1000 **Bosch, M., Serras, F., Martín-Blanco, E. and Baguñà, J.** (2005). JNK signaling pathway required for wound healing in
1001 regenerating Drosophila wing imaginal discs. *Dev Biol* **280**, 73–86.

1002 **Bosch, M., Bagun, J. and Serras, F.** (2008). Origin and proliferation of blastema cells during regeneration of
1003 Drosophila wing imaginal discs. *Int J Dev Biol* **52**, 1043–1050.

1004 **Bose, A., Schuster, K., Kodali, C., Sonam, S. and Smith-Bolton, R. K.** (2025). The pioneer transcription factor Zelda
1005 controls the exit from regeneration and restoration of patterning in *Drosophila*. *Sci Adv* **11**,.

1006 **Brandão, A. S., Borbinha, J., Pereira, T., Brito, P. H., Lourenço, R., Bensimon-Brito, A. and Jacinto, A.** (2022). A
1007 regeneration-triggered metabolic adaptation is necessary for cell identity transitions and cell cycle re-entry to
1008 support blastema formation and bone regeneration. *Elife* **11**,.

1009 **Brown, B., Mitra, S., Roach, F. D., Vasudevan, D. and Ryoo, H. D.** (2021). The transcription factor Xrp1 is required
1010 for PERK-mediated antioxidant gene induction in Drosophila. *Elife* **10**,.

1011 **Bunker, B. D., Nellimoottil, T. T., Boileau, R. M., Classen, A. K. and Bilder, D.** (2015). The transcriptional response
1012 to tumorigenic polarity loss in Drosophila. *Elife* **4**,.

1013 **Choi, H. M. T., Schwarzkopf, M., Fornace, M. E., Acharya, A., Artavanis, G., Stegmaier, J., Cunha, A. and Pierce, N.**
1014 **A.** (2018). Third-generation *in situ* hybridization chain reaction: multiplexed, quantitative, sensitive, versatile,
1015 robust. *Development* **145**,.

1016 **Classen, A.-K., Bunker, B. D., Harvey, K. F., Vaccari, T. and Bilder, D.** (2009). A tumor suppressor activity of
1017 Drosophila Polycomb genes mediated by JAK-STAT signaling. *Nat Genet* **41**, 1150–5.

1018 **Colombani, J., Andersen, D. S. and Léopol, P.** (2012). Secreted peptide dilp8 coordinates Drosophila tissue growth
1019 with developmental timing. *Science (1979)* **336**, 582–585.

1020 **De La Cova, C., Abril, M., Bellosta, P., Gallant, P. and Johnston, L. A.** (2004). Drosophila myc regulates organ size by
1021 inducing cell competition. *Cell* **117**, 107–116.

1022 **De La Cova, C., Senoo-Matsuda, N., Ziosi, M., Wu, D. C., Bellosta, P., Quinzii, C. M. and Johnston, L. A.** (2014).
1023 Supercompetitor status of drosophila Myc cells requires p53 as a Fitness sensor to reprogram metabolism and
1024 promote viability. *Cell Metab* **19**, 470–483.

1025 **Ekas, L. A., Baeg, G.-H., Flaherty, M. S., Ayala-Camargo, A. and Bach, E. A.** (2006). JAK/STAT signaling promotes
1026 regional specification by negatively regulating *wingless* expression in *Drosophila*. *Development* **133**, 4721–
1027 4729.

1028 **Floc'hlay, S., Balaji, R., Stanković, D., Christiaens, V. M., Bravo González-Blas, C., De Winter, S., Hulselmans, G. J.,**
1029 **De Waegeneer, M., Quan, X., Koldere, D., et al.** (2023). Shared enhancer gene regulatory networks between
1030 wound and oncogenic programs. *Elife* **12**,.

1031 **Fox, D. T., Cohen, E. and Smith-Bolton, R.** (2020). Model systems for regeneration: *Drosophila*. *Development* **147**,.

1032 **Garelli, A., Gontijo, A. M., Miguela, V., Caparros, E. and Dominguez, M.** (2012). Imaginal discs secrete insulin-like
1033 peptide 8 to mediate plasticity of growth and maturation. *Science (1979)* **336**, 579–582.

1034 **Germani, F., Hain, D., Sternlicht, D., Moreno, E. and Basler, K.** (2018). The Toll pathway inhibits tissue growth and
1035 regulates cell fitness in an infection-dependent manner. *Elife* **7**,.

1036 **Gouge, C. A. and T.W. Christensen** (2010). Technique Notes-Detection of S Phase in multiple Drosophila tissues
1037 utiliizing the EdU labeling technique. *Drosoph Inf Serv* **93**, 203.

1038 **Gratz, S., O'Connor-Giles, K. M. and Wildonger, J.** (2024). Generating CRISPR Alleles in Drosophila. *Cold Spring Harb*
1039 *Protoc* **2024**, 108256.

1040 **Grewal, S. S., Li, L., Orian, A., Eisenman, R. N. and Edgar, B. A.** (2005). Myc-dependent regulation of ribosomal RNA
1041 synthesis during Drosophila development. *Nat Cell Biol* **7**, 295–302.

1042 **Grusche, F. A., Degoutin, J. L., Richardson, H. E. and Harvey, K. F.** (2011). The Salvador/Warts/Hippo pathway
1043 controls regenerative tissue growth in Drosophila melanogaster. *Dev Biol* **350**, 255–266.

1044 **Hackney, J. F., Pucci, C., Naes, E. and Dobens, L.** (2007). Ras signaling modulates activity of the ecdysone receptor
1045 EcR during cell migration in the drosophila ovary. *Developmental Dynamics* **236**, 1213–1226.

1046 **Hadorn, E. and Buck, D.** (1962). Über entwicklungsleistungen transplantierter teilstücke von flügel-imaginalscheiben
1047 von Drosophila melanogaster. *Revue suisse de Zoologie*.

1048 **Halme, A., Cheng, M. and Hariharan, I. K.** (2010). Retinoids Regulate a Developmental Checkpoint for Tissue
1049 Regeneration in Drosophila. *Current Biology* **20**, 458–463.

1050 **Harris, R. E., Setiawan, L., Saul, J. and Hariharan, I. K.** (2016). Localized epigenetic silencing of a damage-activated
1051 WNT enhancer limits regeneration in mature Drosophila imaginal discs. *Elife* **5**,.

1052 **Harris, R. E., Stinchfield, M. J., Nystrom, S. L., McKay, D. J. and Hariharan, I. K.** (2020). Damage-responsive, maturity-
1053 silenced enhancers regulate multiple genes that direct regeneration in drosophila. *Elife* **9**, 1–26.

1054 **Hazelrigg, T., Levis, R. and Rubin, G. M.** (1984). Transformation of white locus DNA in Drosophila: Dosage
1055 compensation, zeste interaction, and position effects. *Cell* **36**, 469–481.

1056 **Hegedűs, K., Takáts, S., Boda, A., Jipa, A., Nagy, P., Varga, K., Kovács, A. L. and Juhász, G.** (2016). The Ccz1-Mon1-
1057 Rab7 module and Rab5 control distinct steps of autophagy. *Mol Biol Cell* **27**, 3132–3142.

1058 **Herrera, S. C., Martín, R. and Morata, G.** (2013). Tissue Homeostasis in the Wing Disc of Drosophila melanogaster:
1059 Immediate Response to Massive Damage during Development. *PLoS Genet* **9**, e1003446.

1060 **Hirose, K., Shiomi, T., Hozumi, S. and Kikuchi, Y.** (2014). Mechanistic target of rapamycin complex 1 signaling
1061 regulates cell proliferation, cell survival, and differentiation in regenerating zebrafish fins. *BMC Dev Biol* **14**, 42.

1062 **Jaszczak, J. S. and Halme, A.** (2016). Arrested development: coordinating regeneration with development and
1063 growth in Drosophila melanogaster. *Curr Opin Genet Dev* **40**, 87–94.

1064 **Jaszczak, J. S., Wolpe, J. B., Dao, A. Q. and Halme, A.** (2015). Nitric Oxide Synthase Regulates Growth Coordination
1065 During *Drosophila melanogaster* Imaginal Disc Regeneration. *Genetics* **200**, 1219–1228.

1066 **Jaszczak, J. S., Wolpe, J. B., Bhandari, R., Jaszczak, R. G. and Halme, A.** (2016). Growth Coordination During
1067 *Drosophila melanogaster* Imaginal Disc Regeneration Is Mediated by Signaling Through the Relaxin Receptor
1068 Lgr3 in the Prothoracic Gland. *Genetics* **204**, 703–709.

1069 **Johnston, L. A., Prober, D. A., Edgar, B. A., Eisenman, R. N. and Gallant, P.** (1999). Drosophila myc regulates cellular
1070 growth during development. *Cell* **98**, 779–790.

1071 **Karanja, F., Sahu, S., Weintraub, S., Bhandari, R., Jaszczak, R., Sitt, J. and Halme, A.** (2022). Ecdysone exerts biphasic
1072 control of regenerative signaling, coordinating the completion of regeneration with developmental
1073 progression. *Proceedings of the National Academy of Sciences* **119**,.

1074 **Katsuyama, T., Comoglio, F., Seimiya, M., Cabuy, E. and Paro, R.** (2015). During *Drosophila* disc regeneration,
1075 JAK/STAT coordinates cell proliferation with Dilp8-mediated developmental delay. *Proceedings of the National*
1076 *Academy of Sciences* **112**,.

1077 **Khan, S. J., Abidi, S. N. F., Skinner, A., Tian, Y. and Smith-Bolton, R. K.** (2017). *The Drosophila Duox maturation factor*
1078 *is a key component of a positive feedback loop that sustains regeneration signaling*.

1079 **Khandekar, A. and Ellis, S. J.** (2024). An expanded view of cell competition. *Development* **151**,.

1080 **Kiparaki, M. and Baker, N. E.** (2023). Protocol for assessing translation in living Drosophila imaginal discs by O-
1081 propargyl-puromycin incorporation. *STAR Protoc* **4**, 102653.

1082 **Kiparaki, M., Khan, C., Folgado-Marco, V., Chuen, J., Moulos, P. and Baker, N. E.** (2022). The transcription factor
1083 Xrp1 orchestrates both reduced translation and cell competition upon defective ribosome assembly or
1084 function. *Elife* **11**,.

1085 **Kojima, T., Sato, M. and Saigo, K.** (2000). Formation and specification of distal leg segments in *Drosophila* by dual
1086 *Bar* homeobox genes, *BarH1* and *BarH2*. *Development* **127**, 769–778.

1087 **Kudron, M. M., Victorsen, A., Gevirtzman, L., Hillier, L. W., Fisher, W. W., Vafeados, D., Kirkey, M., Hammonds, A.**
1088 **S., Gersch, J., Ammouri, H., et al.** (2018). The ModERN Resource: Genome-Wide Binding Profiles for Hundreds
1089 of *Drosophila* and *Caenorhabditis elegans* Transcription Factors. *Genetics* **208**, 937–949.

1090 **Kuo, Y., Huang, H., Cai, T. and Wang, T.** (2015). Target of rapamycin complex 2 regulates cell growth via Myc in
1091 drosophila. *Sci Rep* **5**, 1–10.

1092 **Ledru, M., Clark, C. A., Brown, J., Verghese, S., Ferrara, S., Goodspeed, A. and Su, T. T.** (2022). Differential gene
1093 expression analysis identified determinants of cell fate plasticity during radiation-induced regeneration in
1094 Drosophila. *PLoS Genet* **18**, e1009989.

1095 **Lee, C.-H., Rimesso, G., Reynolds, D. M., Cai, J. and Baker, N. E.** (2016). Whole-Genome Sequencing and iPLEX
1096 MassARRAY Genotyping Map an EMS-Induced Mutation Affecting Cell Competition in *Drosophila*
1097 *melanogaster*. *G3 Genes|Genomes|Genetics* **6**, 3207–3217.

1098 **Lee, C.-H., Kiparaki, M., Blanco, J., Folgado, V., Ji, Z., Kumar, A., Rimesso, G. and Baker, N. E.** (2018). A Regulatory
1099 Response to Ribosomal Protein Mutations Controls Translation, Growth, and Cell Competition. *Dev Cell* **46**,
1100 456-469.e4.

1101 **Levayer, R., Hauert, B. and Moreno, E.** (2015). Cell mixing induced by myc is required for competitive tissue invasion
1102 and destruction. *Nature* **524**, 476–480.

1103 **Li, W. and Baker, N. E.** (2007). Engulfment Is Required for Cell Competition. *Cell* **129**, 1215–1225.

1104 **Londono, R., Sun, A. X., Tuan, R. S. and Lozito, T. P.** (2018). Tissue Repair and Epimorphic Regeneration: an Overview.
1105 *Curr Pathobiol Rep* **6**, 61–69.

1106 **Mauvezin, C., Ayala, C., Braden, C. R., Kim, J. and Neufeld, T. P.** (2014). Assays to monitor autophagy in Drosophila.
1107 *Methods* **68**, 134–139.

1108 **Merino, M. M., Rhiner, C., Lopez-Gay, J. M., Buechel, D., Hauert, B. and Moreno, E.** (2015). Elimination of Unfit
1109 Cells Maintains Tissue Health and Prolongs Lifespan. *Cell* **160**, 461–476.

1110 **Meyer, S. N., Amoyel, M., Bergantiños, C., De La Cova, C., Schertel, C., Basler, K. and Johnston, L. A.** (2014). An
1111 ancient defense system eliminates unfit cells from developing tissues during cell competition. *Science (1979)*
1112 **346**,.

1113 **Morata, G.** (2021). Cell competition: A historical perspective. *Dev Biol* **476**, 33–40.

1114 **Nagata, R. and Igaki, T.** (2024). Cell competition: emerging signaling and unsolved questions. *FEBS Lett* **598**, 379–
1115 389.

1116 **Nagata, R., Nakamura, M., Sanaki, Y. and Igaki, T.** (2019). Cell Competition Is Driven by Autophagy. *Dev Cell* **51**, 99-
1117 112.e4.

1118 **Nechiporuk, A. and Keating, M. T.** (2002). A proliferation gradient between proximal and msxb-expressing distal
1119 blastema directs zebrafish fin regeneration. *Development* **129**, 2607–2617.

1120 **Ng, M., Diaz-Benjumea, F. J. and Cohen, S. M.** (1995). *nubbin* encodes a POU-domain protein required for proximal-
1121 distal patterning in the *Drosophila* wing. *Development* **121**, 589–599.

1122 **O'Brochta, D. A. and Bryant, P. J.** (1987). Distribution of S-phase cells during the regeneration of Drosophila imaginal
1123 wing discs. *Dev Biol* **119**, 137–142.

1124 **Ochi, N., Nakamura, M., Nagata, R., Wakasa, N., Nakano, R. and Igaki, T.** (2021). Cell competition is driven by Xrp1-
1125 mediated phosphorylation of eukaryotic initiation factor 2α. *PLoS Genet* **17**, e1009958.

1126 **Oldham, S., Montagne, J., Radimerski, T., Thomas, G. and Hafen, E.** (2000). Genetic and biochemical
1127 characterization of dTOR, the *Drosophila* homolog of the target of rapamycin. *Genes Dev* **14**, 2689–2694.

1128 **Parisi, F., Riccardo, S., Daniel, M., Saqcena, M., Kundu, N., Pession, A., Grifoni, D., Stocker, H., Tabak, E. and**
1129 **Bellosta, P.** (2011). Drosophila insulin and target of rapamycin (TOR) pathways regulate GSK3 beta activity to
1130 control Myc stability and determine Myc expression in vivo. *BMC Biol* **9**, 65.

1131 **Paul, P. K., Umarvaish, S., Bajaj, S., S., R. F., Mohan, H., Annaert, W. and Chaudhary, V.** (2024). Maintenance of
1132 proteostasis by Drosophila Rer1 is essential for competitive cell survival and Myc-driven overgrowth. *PLoS*
1133 *Genet* **20**, e1011171.

1134 **Rai, M., Carter, S. M., Shefali, S. A., Chawla, G. and Tennessen, J. M.** (2024). Characterization of genetic and
1135 molecular tools for studying the endogenous expression of Lactate dehydrogenase in Drosophila melanogaster.
1136 *PLoS One* **19**, e0287865.

1137 **Rhiner, C., López-Gay, J. M., Soldini, D., Casas-Tinto, S., Martín, F. A., Lombardía, L. and Moreno, E.** (2010). Flower
1138 forms an extracellular code that reveals the fitness of a cell to its neighbors in Drosophila. *Dev Cell* **18**, 985–
1139 998.

1140 **Rodrigues, A. B., Zoranovic, T., Ayala-Camargo, A., Grewal, S., Reyes-Robles, T., Krasny, M., Christine Wu, D.,**
1141 **Johnston, L. A. and Bach, E. A.** (2012). Activated STAT regulates growth and induces competitive interactions
1142 independently of Myc, Yorkie, Wingless and ribosome biogenesis. *Development (Cambridge)* **139**, 4051–4061.

1143 **Romero-Pozuelo, J., Demetriades, C., Schroeder, P. and Teleman, A. A.** (2017). CycD/Cdk4 and Discontinuities in
1144 Dpp Signaling Activate TORC1 in the Drosophila Wing Disc. *Dev Cell* **42**, 376-387.e5.

1145 **S Bruce, H., Jerz, G., R Kelly, S., McCarthy, J., Pomerantz, A., Senevirathne, G., Sherrard, A., A Sun, D., Wolff, C. and**
1146 **H Patel, N.** (2021). Hybridization Chain Reaction (HCR) In Situ Protocol v1.

1147 **Santabárbara-Ruiz, P., López-Santillán, M., Martínez-Rodríguez, I., Binagui-Casas, A., Pérez, L., Milán, M.,**
1148 **Corominas, M. and Serras, F.** (2015). ROS-Induced JNK and p38 Signaling Is Required for Unpaired Cytokine
1149 Activation during Drosophila Regeneration. *PLoS Genet* **11**, e1005595.

1150 **Serras, F. and Bellosta, P.** (2024). Drosophila: a Tale of regeneration with MYC. *Front Cell Dev Biol* **12**,.

1151 **Shiga, Y., Tanaka-Matakatsu, M. and Hayashi, S.** (1996). A nuclear GFP/β-galactosidase fusion protein as a marker
1152 for morphogenesis in living *Drosophila*. *Dev Growth Differ* **38**, 99–106.

1153 **Smith-Bolton, R. K., Worley, M. I., Kanda, H. and Hariharan, I. K.** (2009). Regenerative Growth in Drosophila Imaginal
1154 Discs Is Regulated by Wingless and Myc. *Dev Cell* **16**, 797–809.

1155 **Sun, G. and Irvine, K. D.** (2011). Regulation of Hippo signaling by Jun kinase signaling during compensatory cell
1156 proliferation and regeneration, and in neoplastic tumors. *Dev Biol* **350**, 139–151.

1157 **Swarup, S. and Verheyen, E. M.** (2012). Wnt/Wingless Signaling in Drosophila. *Cold Spring Harb Perspect Biol* **4**,
1158 a007930–a007930.

1159 **Teleman, A. A., Hietakangas, V., Sayadian, A. C. and Cohen, S. M.** (2008). Nutritional Control of Protein Biosynthetic
1160 Capacity by Insulin via Myc in Drosophila. *Cell Metab* **7**, 21–32.

1161 **Terriente, J., Perea, D., Suzanne, M. and Díaz-Benjumea, F. J.** (2008). The Drosophila gene zfh2 is required to
1162 establish proximal-distal domains in the wing disc. *Dev Biol* **320**, 102–112.

1163 **Terry, D., Schweibenz, C. and Moberg, K.** (2024). Local Ecdysone synthesis in a wounded epithelium sustains
1164 developmental delay and promotes regeneration in *Drosophila*. *Development* **151**,.

1165 **Thummel, C. S.** (2001). Molecular Mechanisms of Developmental Timing in C. elegans and Drosophila. *Dev Cell* **1**,
1166 453–465.

1167 **Tran, K. D., Miller, M. R. and Doe, C. Q.** (2010). Recombineering Hunchback identifies two conserved domains
1168 required to maintain neuroblast competence and specify early-born neuronal identity. *Development* **137**,
1169 1421–1430.

1170 **Venken, K. J. T., Schulze, K. L., Haelterman, N. A., Pan, H., He, Y., Evans-Holm, M., Carlson, J. W., Levis, R. W.,**
1171 **Spradling, A. C., Hoskins, R. A., et al.** (2011a). MiMIC: a highly versatile transposon insertion resource for
1172 engineering Drosophila melanogaster genes. *Nat Methods* **8**, 737–43.

1173 **Venken, K. J. T., Schulze, K. L., Haelterman, N. A., Pan, H., He, Y., Evans-Holm, M., Carlson, J. W., Levis, R. W.,**
1174 **Spradling, A. C., Hoskins, R. A., et al.** (2011b). MiMIC: a highly versatile transposon insertion resource for
1175 engineering Drosophila melanogaster genes. *Nat Methods* **8**, 737–743.

1176 **Worley, M. I., Alexander, L. A. and Hariharan, I. K.** (2018). CtBP impedes JNK- and Upd/STAT-driven cell fate
1177 misspecifications in regenerating Drosophila imaginal discs. *Elife* **7**,.

1178 **Worley, M. I., Everetts, N. J., Yasutomi, R., Chang, R. J., Saretha, S., Yosef, N. and Hariharan, I. K.** (2022). Ets21C
1179 sustains a pro-regenerative transcriptional program in blastema cells of Drosophila imaginal discs. *Current*
1180 *Biology* **32**, 3350-3364.e6.

1181 **Xiao, G., Li, X., Yang, H., Zhang, R., Huang, J., Tian, Y., Nie, M. and Sun, X.** (2024). mTOR mutation disrupts larval
1182 zebrafish tail fin regeneration via regulating proliferation of blastema cells and mitochondrial functions. *J*
1183 *Orthop Surg Res* **19**, 321.

1184 **Yamamoto-Hino, M., Muraoka, M., Kondo, S., Ueda, R., Okano, H. and Goto, S.** (2015). Dynamic regulation of innate
1185 immune responses in *Drosophila* by Senju-mediated glycosylation. *Proceedings of the National Academy of*
1186 *Sciences* **112**, 5809–5814.

1187 **Zhulyn, O., Rosenblatt, H. D., Shokat, L., Dai, S., Kuzuoglu-Öztürk, D., Zhang, Z., Ruggero, D., Shokat, K. M. and**
1188 **Barna, M.** (2023). Evolutionarily divergent mTOR remodels translatome for tissue regeneration. *Nature* **620**,
1189 163–171.

1190